isvr Institute of Sound and Vibration Research

A Velocity Method for Estimating Dynamic Strain and Stress in Pipes

S. Finnveden and R.J. Pinnington

ISVR Technical Report No 274

February 1998

University of Southampton

SCIENTIFIC PUBLICATIONS BY THE ISVR

Technical Reports are published to promote timely dissemination of research results by ISVR personnel. This medium permits more detailed presentation than is usually acceptable for scientific journals. Responsibility for both the content and any opinions expressed rests entirely with the author(s).

Technical Memoranda are produced to enable the early or preliminary release of information by ISVR personnel where such release is deemed to the appropriate. Information contained in these memoranda may be incomplete, or form part of a continuing programme; this should be borne in mind when using or quoting from these documents.

Contract Reports are produced to record the results of scientific work carried out for sponsors, under contract. The ISVR treats these reports as confidential to sponsors and does not make them available for general circulation. Individual sponsors may, however, authorize subsequent release of the material.

UNIVERSITY OF SOUTHAMPTON

INSTITUTE OF SOUND AND VIBRATION RESEARCH

DYNAMICS GROUP

A Velocity Method for Estimating Dynamic Strain and Stress in Pipes

by

S. Finnveden and R.J. Pinnington

ISVR Technical Report No. 274

February 1998

Authorized for issue by
Dr M J Brennan
Group Chairman

ABSTRACT

A velocity method for estimating strain and stress in pipe structures is investigated. With this method predicted or measured spatial average vibration velocity and theoretically derived strain factors are used to estimate maximum strain. The strain in a point is limited by an expression proportional to the square root of the strain energy density which in turn is related to its cross sectional average. For reverberant field or for infinite pipes, the average strain energy density is proportional to the mean square velocity. Upon this basis, the non dimensional strain factor is defined as the maximum strain times the ratio of the sound velocity to the spatial rms vibration velocity. Measurements are made confirming that this is a descriptive number. Using a spectral finite element method, numerical experiments are made varying the pipe parameters and considering all sixteen possible homogenous boundary conditions. While indicating possible limitations of the method when equipment is mounted on pipes, the experiments verify the theoretical results. The velocity method may become useful in engineering practise for assessments of fatigue life.

1. INTRODUCTION

Vibrations in pipes are excited by mechanical machinery, by pumps and by internal turbulent fluid motion. Pipe vibrations cause annoying, sometimes hazardous, noise radiation and can cause failure due to fatigue, possibly resulting in economical and environmental disasters.

Predictions of pipe vibrations are made with the finite element method (FEM) with direct methods formulated in the frequency domain, e.g. [1-4] and with statistical energy analysis (SEA) [5-6]. Most of these methods are not yet sufficiently developed to result in commercially available code while the cost, in man and computer time, required for full scale FE calculation makes this methods application to large pipe structures impractical. Additionally, the lack of knowledge of the sources of vibration makes any prediction doubtful. Therefore, measurements are needed to asses pipe structures integrity, this being increasingly interesting as there is a demand for 'life extension' of existing plants.

In chemical industry, energy production and on off shore installations there are often many kilometre's of pipes. Clearly it is impossible to instrument such plants with strain gauges 'everywhere' to find maximum strain or stress to predict fatigue life. A more practical cause of action would instead be to measure vibration amplitudes using portable accelerometer and analyser equipment.

Previously, relations between vibration velocity and strain have been obtained [7-14]. The amazingly simple result is that, within an element the strain is to a fair approximation proportional to the ratio of the vibration velocity to the dilatational (sound) velocity in the elements material. The objective of the present work is to further our understanding of this 'velocity method' for estimating strain and in particular its application to pipe structures.

Hunt initiated the method studying single mode response in rods and beams [7]. He showed that the maximum strain in a rod (at a vibrational node) is equal to the maximum velocity ratio (at an antinode). Within beams with rectangular cross section the maximum strain is a factor of $\sqrt{3}$ larger than the maximum velocity ratio; at a blocked end the maximum strain is increased an additional 40-65% [7]. Ungar considered wave fields in semi-infinite plate and plate-beam structures deriving the strain as a function of the amplitude of an incoming wave [8]. Ungar defined the 'dynamic strain concentration factor' as the ratio of the strain at a restriction (such as a frame) to the average strain within the element. Stearn studied theoretically and experimentally the statistical variability of the strain within plate and cylinder elements in which there is an approximately diffuse field, showing the variation for frequency band averages to be proportional to the square root of the number of modes within the band [9]. Stearn also calculated and measured the strain concentration at junctions between plate elements with different wall thickness' [10]. Norton and Fahy made measurements on an oil-filled pipe verifying, also for such structures, the simple relation between vibrational strain and radial velocity [11]. However, at a restriction, a flange, the measured strain concentration factor was very large - of the order of 10-100. Possibly so, as the strain at the flange was compared to the velocity at the same place, that is, not to the vibrations within the pipe. Koss and Karczub developed a more elaborated version of the velocity

method [12]. Accelerometer readings were used to find the amplitudes of the four, presumably known, wave solutions to the beam equations and from this the strain was calculated. Recently, Karczub [13] and Karczub and Norton [14] have reviewed and developed the velocity method for predicting strain.

In the present work an alternative theoretical approach to the method is developed based on considerations of vibration energy. The maximum strain, and stress, in a point is related to the strain energy density which, in turn, is limited by a constant factor times its cross sectional average. This gives a foundation for arguing that the maximum strain, being proportional to the strain energy, should be proportional to the average kinetic energy, thus, proportional to the average vibration velocity in the pipe. This approach relating the maximum strain to the average vibration differs, somewhat, from the one in [8-10] where the maximum strain is related to the wave amplitude of incoming waves and, to a greater extent, from the one in [7, 14] where the maximum strain is related to the maximum vibration amplitude. It is argued that the energy approach can be conceptually more productive, that the relation to results from SEA calculations is more direct and that it is practically simpler to measure average vibration than to find the maximum vibration amplitude.

In Section 3 measurements on a pipe structure with a blocked end are presented. The results agree with those by Karczub and Norton [14] but for a factor $\sqrt{2}$ - a possible explanation for this difference is given. The measurement results are compared to those found with the direct dynamic finite element method presented in [4], here developed by routines for calculating average vibration response and for calculating strain and stress. The good agreement of the results justifies the numerical approach for simulating vibration velocity and strain.

In Section 4, numerical experiments are presented. Dimensional analysis shows that the vibration of pipes is a function of only a few non-dimensional numbers. By varying these and the boundary conditions, sixteen in all, a fairly comprehensive investigation is made of the relation between average radial velocity and maximum strain in pipes. The results show the potential for the velocity method for assessing fatigue of pipe structures. However, they also point on a possible limitation for special boundary conditions.

2. MAXIMUM STRAIN AND STRESS IN CYLINDERS

In this section the stress and strain in cylinders are expressed. Limits for their maxima are found to be proportional to the square root of the strain energy density. For reverberant fields or in wave fields, the strain energy density is related to the average vibration energy. It is argued, the average vibration energy is estimated by the average radial vibration velocity, which is accessible from comparatively simple measurements.

The motion of the cylinder is described with an implicit time dependence of the form $e^{-i\omega t}$. Thus the analysis applies for harmonic vibration and stationary random vibration.

2.1 STRAIN AND STRESS IN CYLINDERS

The motion of thin-walled cylinders is investigated using a Fourier decomposition of the circumferential dependence of the displacements and using the Kirchhoff hypothesis [15]. Thus, the strains, in directions specified in Figure 1, are

$$\gamma_{xz} = \gamma_{\phi z} = \gamma_z = 0, \tag{1}$$

while the displacements are

$$u_x = (u + z\theta_1)\cos(n\phi);\ u_\phi = (v + z\theta_2)\sin(n\phi);\ u_z = w\cos(n\phi), \tag{2}$$

where, from equation (1)

$$\theta_1 = -\frac{\partial w}{\partial x};\ \theta_2 = (v + nw)/R. \tag{3}$$

Using the Love-Timoshenko strain-displacement relations for thin-walled cylinders, neglecting all but the dominating terms in the small quantity T_c / R, the remaining three strain components are [16]

$$\gamma_x = (\varepsilon_x + z\kappa_1)\cos(n\phi);\ \gamma_\phi = (\varepsilon_\phi + z\kappa_2)\cos(n\phi);\ \gamma_{x\phi} = (\gamma + z\tau)\sin(n\phi), \tag{4}$$

where T_c is the cylinder wall thickness and R is the radius and where

$$\begin{gathered} \varepsilon_x = \frac{\partial u}{\partial x};\ \varepsilon_\phi = \frac{nv + w}{R};\ \gamma = -\frac{nu}{R} + \frac{\partial v}{\partial x}; \\ \kappa_1 = -\frac{\partial^2 w}{\partial x^2};\ \kappa_2 = \frac{nv + n^2 w}{R^2};\ \tau = \frac{2}{R}\left(\frac{\partial v}{\partial x} + n\frac{\partial w}{\partial x}\right). \end{gathered} \tag{5}$$

Accordingly, considering an isotropic Hookean material and assuming plane stress [15, p. 14], the stresses are

$$\sigma_x = E'(\gamma_x + \nu\gamma_\phi), \quad \sigma_\phi = E'(\gamma_\phi + \nu\gamma_x), \quad \sigma_{x\phi} = G\gamma_{x\phi}, \tag{6}$$

where

$$E' = E/(1-\nu^2), \quad G = E/2(1+\nu), \tag{7}$$

and where E is Young's modulus and ν is Poisson's ratio.

The state of stress in a point is given by the stress tensor, **S** [17],

$$\mathbf{S} = \begin{bmatrix} \sigma_x & \sigma_{x\phi} \\ \sigma_{x\phi} & \sigma_\phi \end{bmatrix} = \Phi * \begin{bmatrix} \sigma_1 & 0 \\ 0 & \sigma_2 \end{bmatrix} * \Phi^T, \tag{8}$$

where the last equality follows from an eigenvalue decomposition of **S**. Thus, σ_i are the eigenvalues and the eigenvectors are the columns of Φ. From this, it follows that if the stress is expressed in the coordinate system given by the stress tensor's eigenvectors, the shear stress vanishes and the stresses in these coordinates, the principal stresses, are the eigenvalues of **S**, σ_1 and σ_2. We will assume that

$$|\sigma_1| \geq |\sigma_2|. \tag{9}$$

Similarly, the strain in a point is given by the strain tensor

$$\mathbf{s} = \begin{bmatrix} \gamma_x & \gamma_{x\phi}/2 \\ \gamma_{x\phi}/2 & \gamma_\phi \end{bmatrix}. \tag{10}$$

For an Hookean material the directions of principal stress and principal strain coincide. Expressed in a coordinate system in these directions the shear strain vanishes and the principal strains are γ_1 and γ_2. From equations (6) and (9), for an isotropic material

$$|\gamma_1| \geq |\gamma_2|. \tag{11}$$

The maximum stress in a point is σ_1. An upper bound to $|\sigma_1|$ is given by

$$\begin{aligned} |\sigma_1| &= E'|\gamma_1 + \nu\gamma_2| = E'\sqrt{|\gamma_1|^2 + 2\nu\,\mathrm{Re}(\gamma_1^*\gamma_2) + |\nu\gamma_2|^2} \\ &\leq E'\sqrt{|\gamma_1|^2 + 2\nu\,\mathrm{Re}(\gamma_1^*\gamma_2) + |\gamma_2|^2} = \sqrt{E'\,2\,e_p}, \end{aligned} \tag{12}$$

where γ_1^* denotes the complex conjugate of γ_1 and where e_p is the strain energy density [15, equation (1.85)]. The strain energy density is invariant to coordinate transformations, hence it is equally expressed in the cylinder coordinate system

$$e_p = E'/2\left(\gamma_x\gamma_x^* + \nu\left(\gamma_x\gamma_\phi^* + \gamma_\phi\gamma_x^*\right) + \gamma_\phi\gamma_\phi^* + g\gamma_{x\phi}\gamma_{x\phi}^*\right), \tag{13}$$

where

$$g = G/E' = 2/(1+\nu). \tag{14}$$

To find a similar limit for the maximum principle strain, it is easier to go backwards

$$\begin{aligned} 2e_p/E' &= |\gamma_1 + \nu\gamma_2|^2 + (1-\nu^2)|\gamma_2|^2 \geq \\ (|\gamma_1| - \nu|\gamma_2|)^2 + (1-\nu^2)|\gamma_2|^2 &= |\gamma_1|^2\left(1 - 2\nu|\gamma_2/\gamma_1| + |\gamma_2/\gamma_1|^2\right). \end{aligned} \tag{15}$$

This function has a minimum at $|\gamma_2| = \nu|\gamma_1|$, from which it follows that

$$|\gamma_1| \leq \sqrt{\frac{2e_p}{(1-\nu^2)E'}} = \sqrt{2e_p/E'}. \tag{16}$$

So, limits for the maximum strain and stress have been found. These limits may be used for estimates. The possible overestimation that such a procedure results in is found as in equation (15)

$$2e_p/E' \leq (|\gamma_1| + \nu|\gamma_2|)^2 + (1-\nu^2)|\gamma_2|^2 = |\gamma_1|^2\left(1 + 2\nu|\gamma_2/\gamma_1| + |\gamma_2/\gamma_1|^2\right). \tag{17}$$

Since by definition $|\gamma_2| \leq |\gamma_1|$ this function is maximised for $|\gamma_2| = |\gamma_1|$. Therefore

$$|\gamma_1| \leq \sqrt{2e_p/E} \leq |\gamma_1|\sqrt{2/(1-\nu)}. \tag{18a}$$

By similar calculations

$$|\sigma_1| \leq \sqrt{2e_pE'} \leq |\sigma_1|\sqrt{2/(1-\nu)}. \tag{18b}$$

For an isotropic material $0 \leq \nu \leq 0.5$. Hence, using equations (12) and (15) for estimating strain and stress may lead to an overestimation by a factor of two. This maximum overestimate results for $\nu = 0.5$ and if the two principal strains (stresses) are equally large.

2.2 Maximum cross-sectional strain energy

Above, limits for the maximum stress and strain in a point are expressed as functions of the strain energy density. In this section, the points, on the cylinder cross-section, where the strain energy is maximised are identified and limits for these maxima are found to be proportional to the cross sectional average of the strain energy density.

As in equations (2) and (6), the strain and stress are linearly varying functions of z and consequently the maxima for strain and stress are at either of $z = \pm T_c / 2$.

The value of ϕ for which the strain energy density is maximised is found when it is recognised, see equations (4) and (13), that this function can be expressed

$$e_p(x,\phi,\pm Tc/2) \;=\; C_1(x)\cos^2(n\phi)+C_2(x)\sin^2(n\phi). \tag{19}$$

Dependent on the values of the (unknown) positive functions C_1 and C_2, the maxima of this function are either where $\cos(n\phi)=0$ or where $\sin(n\phi)=0$. These maxima are

$$\max_\phi\left(e_p(x,\phi,\pm Tc/2)\right) \;=\; \max(C_1, C_2), \tag{20}$$

from which it is concluded that, for each trigonometric order n,

$$e_p(x,\phi,\pm Tc/2) \;\le\; 1/\Lambda_n \;\left\langle e_p(x,\phi,\pm Tc/2)\right\rangle_\phi, \tag{21}$$

where $\langle\ \rangle_\phi$ denotes averaging over ϕ and where

$$\Lambda_0 = 1;\quad \Lambda_n = 1/2,\quad n \ge 1. \tag{22}$$

If there are several trigonometric orders present and they are assumed uncorrelated, the estimated value of the maximum e_p is still given by equation (21). However, the maximum possible value of e_p is

$$\max_\phi\left(e_p(x,\phi,\pm Tc/2)\right) \;\le\; N/\Lambda_n \;\left\langle e_p(x,\phi,\pm Tc/2)\right\rangle_\phi, \tag{23}$$

where N is the number of trigonometric orders that are excited. This maximum value result if the strain energy densities of all the trigonometric orders are equal and if they all are maximised at the same value of ϕ, at the same time. This requires fully coherent sources, for example a point source. However, as the different trigonometric orders travels with different velocities their relative phases will vary with frequency, unless the source is very peculiar. Therefore, for broad band excitation that is several wavelengths away it is reasonable to assume the different trigonometric orders incoherent so that equation (21) applies, on average.

It should be remembered, though, that if the trigonometric orders are coupled by the boundary conditions, for instance if the pipe is supported only at one point, equation (23) may apply. In this study, only homogeneous boundary conditions of the first and second kind are considered and these do not couple the trigonometric orders, so equation (21) is tentatively assumed to be valid also for coherent excitation.

Above, limits of maximum strain and stress are expressed as functions of the strain energy density at $z = \pm T_c / 2$ averaged over the circumferential. The next step is to express these limits as functions of the averaged cross-sectional strain energy density. To that end, consider

$$\begin{aligned}\frac{1}{\Lambda_n E^{\cdot}}\left\langle e_p\left(x, \phi, \pm Tc/2\right)\right\rangle_{\phi} &= \left(\left|\varepsilon_x \pm \frac{T_c}{2}\kappa_1\right|^2 + \left|\varepsilon_\phi \pm \frac{T_c}{2}\kappa_2\right|^2\right. \\ &\left. + 2\nu\,\mathrm{Re}\left(\left(\varepsilon_\phi \pm \frac{T_c}{2}\kappa_2\right)^*\left(\varepsilon_x \pm \frac{T_c}{2}\kappa_1\right)\right) + g\left|\gamma \pm \frac{T_c}{2}\tau\right|^2\right) \\ &\le 4\left[\left(|\varepsilon_x|^2 + |\varepsilon_\phi|^2 + 2\nu\,\mathrm{Re}\left(\varepsilon_\phi^{\,*}\,\varepsilon_x\right) + g|\gamma|^2\right)\right. \\ &\left. + \frac{T_c^2}{12}\left(|\kappa_1|^2 + |\kappa_2|^2 + 2\nu\,\mathrm{Re}\left(\kappa_1^{\,*}\,\kappa_2\right) + g|\tau|^2\right)\right] \\ &= \frac{4}{\Lambda_n E^{\cdot}}\left\langle e_p(x, \phi, z)\right\rangle_{\phi,z}.\end{aligned} \tag{24}$$

where the average over z is calculated as in the derivation of the Arnold and Warburton cylinder theory, that is upon neglecting the trapezoidal form of the cylinder cross-section. The factor of four in the in-equality results as for any a and b, $\left|a + \sqrt{3}\,b\right|^2 \le 4\left(|a|^2 + |b|^2\right)$. In equation (24), the left and right hand sides are equal if the in-plane strain is a factor $1/\sqrt{3}$ less than the flexural strain, in each of the four terms. For propagating radial-axial waves, below the ring-frequency this is not the case. For these waves the dominating terms in the strain energy density are the in-plane axial, circumferential flexural and flexural shear [18]. These terms appear in different terms in the left hand side of equation (24). Thus, using the right hand side of the equation for estimating stress, in many cases, leads to an overestimation of a factor in the range of $2/\sqrt{3}$ to 2, as compared to the left hand side. However, the result leads to the beneficial conclusion that the maximum stress in a cross-section of a cylinder is limited by an expression that is proportional to the square root of the cross-sectional average of the strain energy density.

2.3 Distribution of strain and stress along the cylinder

Hamilton's principle states that the true motion of a system is the one that minimise the time averaged difference between potential and kinetic energy. For two important cases this difference is zero. Thus, for a wave in an infinite cylinder the time averages of the kinetic and the potential cross-sectional energy densities, for any x, are equal. Also, for a finite cylinder performing free vibrations and obeying any of the classical boundary conditions (i.e., homogeneous boundary conditions of the first or second kind), the time average total kinetic and potential energies are equal.

The classical boundary conditions are characterised by that there is no work, thus no exchange of energy, at the boundary. For the industrially very important case of a long

pipe (being many wavelengths long) similar 'boundary conditions' may be found within the pipe. At frequencies below half the ring-frequency and above cut-on, for each $n \geq 1$, there are only two real solutions to the dispersion relations for cylinders corresponding to a right and a left going wave respectively. In addition there are 6 solutions corresponding to 'near field' terms. These near field terms are found in the vicinity of the excitation and boundaries, decaying exponentially away from irregularities. This means, within the pipe at a point x being in-between a boundary and the excitation, there are only two waves present. If the boundary condition is conservative and the damping is not large, the amplitudes of these two waves are equal. Consequently, the vibration field in such a point is

$$u = u_n \sin(\lambda_n x + \alpha_n)\cos(n\phi), \quad v = v_n \cos(\lambda_n x + \alpha_n)\sin(n\phi), \tag{25}$$

$$w = w_n \cos(\lambda_n x + \alpha_n)\cos(n\phi),$$

where λ_n is found from the dispersion relations as are the relative amplitudes u_n / w_n and v_n / w_n. The phase constant α_n is governed by the nearest boundary condition, at $x = 0$. The amplitude w_n is determined by the excitation and by the boundary conditions at the other end.

Langley derived expressions for the energy flow in cylindrical shells [19, equations (21)-(29)]. By merely inspecting these expressions, considering a displacement field of the form (25), it is seen that the reactive work in the pipe is zero at the nodes of the radial displacement which are given by

$$\cos(\lambda_n x + \alpha_n) = 0. \tag{26}$$

(If losses are present there will, however, be a small active energy flow to balance the energy dissipation in the pipe between the considered point and the boundary.)

This quite lengthy discussion leads to two interesting conclusions. First, consider a pipe-section in-between the boundary and a nodal point, as given by equation (25) and being at least one or two wavelengths away from the boundary. Such a pipe section is from a reactive point of view energetically isolated from the rest of the pipe. Thus, Hamilton's principle applies for this section and the average potential and kinetic energies are equal. Second, for the vibration field in such a section, the excitation and the boundary conditions at the other end are only reflected by the amplitude of the (comparatively few) incoming waves. Because of this, the concentration of stress at a boundary may be investigated without considering the excitation and the other boundary condition in detail.

2.4 Relating maximum stress to average vibration velocity

In the previous sections, first the maximum strain and stress were found to be limited by expressions proportional to the square root of strain energy density. Then the strain energy density was found to be limited by an expression proportional to its cross sectional average. It was shown that the average strain energy within a pipe section, extending one or a few wavelengths from a boundary, is equal to the average kinetic energy within this section.

Away from the boundary and the excitation and any other irregularities, where the vibration field is as in equation (25), the maximum strain energy is four times its average. It is argued, at a boundary the strain energy may become even larger but this increase must be limited since there is a limited number of boundary conditions to fulfil, giving rise to a limited number of nearfield components resulting in a limited increase in the cross sectional strain energy.

The kinetic energy density in a thin-walled pipe is

$$e_k = \frac{1}{2}\rho\,\omega^2\left(|u|^2+|v|^2+|w|^2\right). \tag{27}$$

For frequencies well below the ring frequency and considering the radial-axial modes ($n \geq 1$), the axial in-plane inertia may be neglected and the cylinder motion is almost inextensional. Then the cross sectional average kinetic energy density, to a good approximation, is proportional to the square of the radial velocity [18]

$$e_k = \frac{1}{4}\rho\,\omega^2|w|^2\left(1+1/n^2\right). \tag{28}$$

Now, from the arguments above, it is hypothesised, the maximum strain at a boundary is given by

$$\left(|\gamma|_{\max}\right)^2 \leq 2\left(e_p\right)_{\max}/E = konst * \rho/E\,\left\langle\omega^2|w|^2\right\rangle, \tag{29}$$

where $\langle\ \rangle$ denotes spatial average and where the non dimensional constant *konst* is dependent on frequency and boundary condition. It may also depend on excitation and the relative amplitudes of the incoming waves of different trigonometric orders in which case the hypothesis is not effective. However, for boundary conditions that are separable in x and ϕ and for pipes where the excitation is several wavelengths away from the boundary, the arguments above support the idea of an effective and descriptive non dimensional number.

Upon this basis, we define the non dimensional strain factor Γ

$$\Gamma = |\gamma|_{\max}\frac{c_L}{V};\quad c_L = \sqrt{E/\rho};\quad V = \sqrt{\left\langle\omega^2 w^2\right\rangle}. \tag{30}$$

Following Hunt [7] it is seen that for a rod $\Gamma = \sqrt{2}$. Within a beam $\Gamma = \sqrt{6}$ whereas at a blocked end of a beam, according to Hunt, it is an additional 40-65% higher. Karzub and Norton published a list for the relation between maximum velocity and strain [14]. Converting the value given for a cylinder to a relation between average velocity and strain gives $\Gamma = 4$.

The rest of this paper is devoted to justify the value of the strain factor with numerical experiments and with measurements. First, in Section 3, a small pipe structure is considered and measurements are presented confirming, roughly, the hypothesis. The measurements are compared with calculations using the spectral finite element method [4] and the good agreements of the results justify the numerical approach. Then, in Section 4, systematic numerical experiments are presented. Semi-infinite, point excited, pipe structures are considered. The non-dimensional parameters that describe pipe vibration are varied and all the classical boundary conditions (sixteen in all) are considered. These experiments show the practicability of the proposed approach. The presented strain concentrations factors Γ may become useful in engineering practice. However, future research is needed to find the strain factors for equipment mounted on pipes.

3 EXPERIMENTS

To verify that the maximum strain in a pipe is proportional to the rms average vibration velocity and to find the constants of proportionality, experiments are made on a pipe. It was expected, the classical boundary condition that causes the largest strain concentration is the one with all displacement components blocked. To facilitate the application of this boundary condition a light-weight plastic (drain) pipe was chosen for the experiments.

In what follows the relation between the average vibration velocity of the pipe and the strain at the blocked end is estimated from measurements. The results are compared to those from calculations with the spectral finite element method presented in [4]. Before this, measurements are made to determine the material data of the plastic pipe. Also, to verify the spectral FE-code, the results of a simple response calculation are compared to measurements.

3.1 PIPE DATA

The wall thickness, radius and density of the pipe were measured using a pair of callipers and a scale. To find the loss factor and Young's modulus, a 2 *cm* long slice of the pipe was cut off. This ring was hung in a thin elastic string and its accelerance was measured using a light weight accelerometer and an impact hammer. In Figure 2 is the transfer accelerance to a point 180 degrees from the force.

The resonance frequencies of a thin-walled ring are given by

$$f_n^2 = \beta \frac{n^2\left(n^2-1\right)^2}{1+n^2} \frac{E/\rho}{(2\pi R)^2} \tag{31}$$

Young's modulus is estimated with a least square fit applying equation (31) to the first three resonances, corresponding to $n = 2$, 3 and 4. As can be seen in Figure 2, there is a slight tendency that the stiffness of the ring increases at higher frequencies. Besides this, the experiment verifies the use of linear thin-walled theory for describing the plastic pipe.

The pipe loss factor is estimated from the rings point mobility using the 3-dB bandwidth for the first four resonance's.

The response calculation, described in Section 3.2 below, was initially made with Poisson's ratio, $\nu = 0.3$. This resulted in slightly too low cut-on frequencies for the higher order radial-axial modes, when compared to measurements. The resonance frequencies for the $n = 1$, beam modes, are almost independent on Poisson's ratio while for the $n \geq 2$ modes, the cut-on frequencies are proportional to $1/\sqrt{1-\nu^2}$ [18]. Using this, an improved estimate of Poisson's ratio is, $\nu = 0.4$.

The data for the pipe thus found are specified in Table 1 and will be used in the calculations.

3.2 PIPE VIBRATION RESPONSE

The plastic pipe was freely hung in two elastic strings. Vibrations were excited by an impact hammer and the acceleration was measured with a light weight accelerometer. To avoid that the low frequency pendulum motion of the pipe should ruin the dynamic range of the measurement, the signals were high pass filtered. The experiment was also simulated with the spectral FE program [4] using a constant frequency resolution of 1 Hz, the same as in the measurements. The calculations were made considering only the pipe, thus neglecting the fluid loading from the air.

Figures 3, 4 and 5 shows the measured and calculated point mobility, input power from the point source and a transfer mobility. At very low frequencies, the frequency resolution is too coarse to accurately display the peak value at resonance. At high frequencies, it appears as if the damping of the laboratory pipe increases, perhaps due to sound radiation. As for the ring, a slight increase of the stiffness at very high frequencies is noticed. Despite these differences, the agreement between measured and calculated vibration response is good enough to justify the spectral FE code.

3.3 STRAIN CONCENTRATION AT A BLOCKED END.

3.3.1 *Measurement procedure*

A 100 *mm* long solid steel cylinder was 'push-fitted' into the plastic pipe and then glued to a heavy plate so that the pipe motion at the end should be blocked. The other end of the pipe was hung in an elastic string.

Vibrations in the pipe were excited with a small coil and magnet vibrator that was fed with pseudo random noise. To get a reasonable signal to noise ratio also at higher frequencies the noise amplitude was, from 100 Hz, increased with 2 dB/octave.

The strain at the blocked end was measured with strain gauges made and developed by Liu and Pinnington [20, 21]. These gauges are made from piezo electric film that is folded so that they are sensitive only to strain in one direction. They have a high sensitivity and good linearity also at higher frequencies. Another advantage is that the signals are conditioned with the same type of charge amplifier that is used for accelerometer measurements; this is convenient and gives a good phase match between measurement channels.

The strain gauges were fitted to the pipe with double sided tape and were screened with aluminium foil on the outside of the pipe. One of the major disadvantages with these gauges is that they are very sensitive to electromagnetic fields and despite the screening the measurements were quite noisy. (In the results shown below, the 50 Hz component is suppressed by setting it to the average of the measured value at 48 Hz and 52 Hz.) Liu calibrated the strain gauges carefully [21]. This calibration was confirmed for one of the gauges by comparison with a standard strain gauge that was glued to the pipe.

Five strain gauges were randomly positioned at the blocked end - three in the axial direction and two in the circumferential direction. Accelerometer positions were chosen at random within a segment of the pipe starting one pipe diameter away from the blocked end and extending approximately one meter towards the excitation. For each of the strain gauges, the transfer functions between strain and acceleration in four

positions were measured. The accelerometers were then moved and the measurements repeated. The eight transfer functions were then integrated, their rms average was calculated and finally the result was inverted so that an estimate of the ratio of the strain to the average vibration velocity was found.

Figure 6 shows a typical accelerometer and strain measurement. Also shown is the coherence which is quite low at frequencies where the strain is small. However, the coherence is good but at the minima of the strain while this work is focused on maximum strain.

Figure 7a shows the strain factor, equation (30), for the three axial and Figure 7b for the two circumferential strain gauges. Figure 8 shows, for each of the three axial strain gauges, the relative standard deviation of the eighth transfer functions between acceleration and strain. The relative standard deviation is of the order of 0.4 showing that, in this experiment, eight accelerometers is just about enough for estimating the average vibration velocity.

The results show that the strain varies with frequency, direction and position, while it is limited. Thus, in all cases the non dimensional strain factor Γ, equation (30), is smaller than approximately five.

3.3.2 *Spectral Finite Element Calculation*

The measurements are simulated with the spectral finite element method (SFEM) [4]. Using this method the element formulation is remade for each frequency. The shape functions are a combination of the solutions to the equations of motion that depends linearly on the displacements at the ends. For a pipe element, between $x=-L$ and $x=L$, the shape functions are

$$\begin{bmatrix} u \\ v \\ w \end{bmatrix} = \begin{bmatrix} \mathbf{B}_u \\ \mathbf{B}_v \\ \mathbf{B}_w \end{bmatrix} * \mathrm{diag}\left(\exp\left(\alpha x - \alpha_p L\right)\right) * \mathbf{A} * \begin{bmatrix} \mathbf{V}_1 & \mathbf{V}_2 \end{bmatrix}^T \tag{32}$$

where the row vectors $\mathbf{B}_u, \mathbf{B}_v$ and $\mathbf{B}_w$ and the wave numbers α are found from the dispersion relations [4]. This means that any of the columns of the 3 by 8 matrix

$$\begin{bmatrix} \mathbf{B}_u \\ \mathbf{B}_v \\ \mathbf{B}_w \end{bmatrix} * \mathrm{diag}\left(\exp(\alpha x)\right) \tag{33}$$

is an exact solution to the homogeneous equations of motion for the pipe.

In equation (32)

$$\alpha_p = -\alpha, \quad \text{if } \mathrm{Re}(\alpha) < 0; \quad \text{otherwise, } \alpha_p = \alpha, \tag{34}$$

and

$$\mathbf{V}_1 = [u(-L) \quad v(-L) \quad w(-L) \quad \partial\, w(-L)/\partial\, x], \tag{35}$$

$$\mathbf{V}_2 = [u(L) \quad v(L) \quad w(L) \quad \partial\, w(L)/\partial\, x],$$

whereas the matrix **A** is governed by the linear equation system resulting when the expression for the shape functions (32) is inserted into the boundary conditions (35).

The response of the pipe is calculated with the SFEM using the shape functions (32) in the element formulation. The excitation is a point force at a distance 2 *m* from the blocked end. Calculations are made for frequencies from 10 Hz up to 3.2 kHz with 2 Hz spacing (the same as in the measurements). The trigonometric orders $n = 0$ to $n = 8$ are considered. The major time consumption when using the SFEM is to calculate the shape functions. Therefore these are stored when the element formulation is made, so that the post processing described below is made efficiently.

3.3.3 *Average radial vibration velocity*

Once the nodal displacements $\mathbf{V}_1$ and $\mathbf{V}_2$ are known, the rms radial vibration velocity in a pipe segment, for the trigonometric order *n*, is given by

$$\left\langle (\omega w)^2 \right\rangle = \frac{\Lambda_n \omega^2}{X_2 - X_1} \int_{X_1}^{X_2} |w|^2 \, \mathrm{dx} = \tag{36}$$

$$\frac{\Lambda_n \omega^2}{X_2 - X_1} \left[\mathbf{V}_1^* \quad \mathbf{V}_2^*\right] \mathbf{A}^{\mathrm{H}} * \mathrm{diag}\left(\mathbf{B}_w^*\right) * \mathbf{E} * \mathrm{diag}\left(\mathbf{B}_w\right) * \mathbf{A} * \left[\mathbf{V}_1 \quad \mathbf{V}_2\right]^T$$

where * denotes complex conjugate, $^{\mathrm{H}}$ denotes complex conjugate and transpose and where the matrix **E** is given by

$$\mathbf{E} = \mathbf{E}(\alpha, X_1, X_2, L) = \int_{X_1}^{X_2} \exp\left(\alpha x - \alpha_p L\right)^H * \exp\left(\alpha x - \alpha_p L\right) \, \mathrm{dx}\,. \tag{37}$$

The integral is calculated explicitly and upon this the $[i, j]$ element of the matrix **E** is

$$\mathbf{E}[i,j] = \frac{\left[\exp\left((\alpha^*[i] + \alpha[j])X_2\right) - \exp\left((\alpha^*[i] + \alpha[j])X_1\right)\right]}{\alpha^*[i] + \alpha[j]} * \exp\left(-\left(\alpha_p{}^*[i] + \alpha_p[j]\right) L\right) \tag{38}$$

3.3.4 *Maximum strain at the blocked end*

Using the standard FEM, because of increasing discretization errors when derivatives of the polynomial shape functions are calculated, the strains are not as accurately

calculated as the displacements. However, with the shape functions (32) the derivatives needed for the strain are calculated explicitly without any errors. Consequently, from equations (4), (5) and (32), the strains are given by

$$\gamma_x(x,\phi,z) = \cos n\phi * \left[\mathbf{B}_u * \mathrm{diag}(\alpha) - z\,\mathbf{B}_w * \mathrm{diag}(\alpha)^2\right] * \mathbf{W}, \tag{39}$$

$$\gamma_\phi(x,\phi,z) = \cos n\phi * \left[(n\mathbf{B}_v + \mathbf{B}_w)/R + z(n\mathbf{B}_v + n^2\mathbf{B}_w)/R^2\right] * \mathbf{W},$$

$$\gamma_{x\phi}(x,\phi,z) = \sin n\phi * \left[-n\mathbf{B}_u/R + \mathbf{B}_v\,\mathrm{diag}(\alpha) - 2z/R\,(\mathbf{B}_v + n\mathbf{B}_w) * \mathrm{diag}(\alpha)\right] * \mathbf{W}$$

where the vector $\mathbf{W}$ is

$$\mathbf{W}(x) = \mathrm{diag}\left(\exp(\alpha x - \alpha_p L)\right) * \mathbf{A} * \left[\mathbf{V}_1 \quad \mathbf{V}_2\right]^T. \tag{40}$$

The strains are calculated at the blocked end on the outside of the pipe, at $z=T_c/2$. The contributions for each trigonometric order $n = 0$ until $n = 8$ are calculated and summed. Then the largest eigenvalue of the strain tensor, equation (10), is calculated. This procedure is repeated for 180 equally spaced angular positions. Finally, the maximum strain at the blocked end of the pipe is found as the maximum of the largest principle strain in any of the 180 points along the circumferential.

3.3.5 *Results*

In Section 2, equation (30), the non dimensional dynamic strain factor Γ was defined as the maximum strain times the ratio of the sound velocity to the spatial rms radial velocity. The calculated dynamic strain factor is plotted in Figure 9. At low frequencies Γ has an approximately constant value: $\Gamma \approx 6$. At very low frequencies it increases somewhat as the part of the pipe where the motion is almost blocked increases with the wavelength and therefore the calculated rms velocity in the section near the boundary becomes smaller. At higher frequencies, when the $n \geq 2$ modes are cut-on, the dynamic strain factor fluctuates. The different trigonometric orders are correlated as the incoming waves originates form the same point source. As the source is several wavelengths away and the trigonometric orders travel with different speed their relative phase varies rapidly with frequency and so does the maximum strain. The fluctuations, however, are not very large and the constant value $\Gamma \approx 6$ still applies on average. At frequencies above 1 kHz, there is a small drop in the strain factor, probably caused by damping. At high frequencies the energy density decays away from the source so that the vibration energy at the blocked end has decayed more than the average energy in the section where the velocity is calculated.

Also plotted in Figure 9 is the measured value of Γ. It is found by taking, for each frequency, the maximum of the five strain factors shown in Figures 7. The measured value fluctuates more than the measured and is consistently lower. There are three possible explanations for the differences: 1) The strain is measured only in one direction at five positions, hence it is very unlikely that the maximum strain in the cross section is detected. Therefore, the measured value should be lower than the calculated. 2) It is in

practise difficult to obtain a truly blocked boundary. Failure to achieve this will probably result in a lower strain factor. 3) The size of the strain gauge is approximately 2 *cm*, so it is impossible to measure the strain exactly at the blocked end. For the considered frequencies there are for each $n \geq 1$ eight solutions to the dispersion relations; two travelling waves (one in each direction), two exponentially decaying nearfield components and four 'standing decaying waves'. These last four corresponds to wave solutions that are cut-off below the ring frequency. At the considered frequencies they have an approximately constant value which for $n = 1$ (having the slowest exponential decay) is: $\alpha \approx \pm 164 \pm i158$. This large value means that within a few centimetres the strain associated with the standing decaying waves has completely vanished. Consequently, a measurement with a finite size strain gauge which is not positioned exactly on the boundary will underestimate the strain.

To investigate this last explanation for the difference between measured and calculated results, the strain factor was calculated 2 *cm* away from the blocked end. Figure 9 shows the measured and the two calculated strain factors, demonstrating that the exact positioning of the strain gauges influences the results. For the investigated pipe, the strain factor decreases approximately a factor $\sqrt{2}$ when a point slightly away from the boundary is considered.

As mentioned in the Introduction, Karzub and Norton have measured the ratio of maximum strain to maximum velocity [14]. They found a constant $K = 2$, which, since the maximum velocity for a pipe is twice the spatial rms value, corresponds to a strain factor $\Gamma = 4$. This is a factor $\sqrt{2}$ lower than the one found theoretically here indicating that a finite size strain gauge was used.

From the experiments it is concluded that the maximum strain in a pipe can be estimated from accelerometer measurements. In addition, the great variability of the strain at the blocked end shows that it is difficult to find the maximum strain at a cross section using strain gauges. In consequence, despite the uncertainty of the exact value of the factor Γ for 'real-life' structures, the velocity method is not only more convenient, it can perhaps also be a more reliable method for finding maximum strain to predict fatigue life.

4 NUMERICAL EXPERIMENTS

Dimensional analysis shows the free vibration of cylinders to be a function of only four non-dimensional numbers

$$\beta = \frac{T_c^2}{12R^2}, \quad \Omega = \frac{\omega R}{c_L}, \; n \text{ and } \nu, \tag{41}$$

where Ω is the non dimensional frequency. Forced vibrations of finite cylinders, in addition to the four non dimensional numbers in equation (41), also depend on the excitation and on the boundary conditions. However, from the analysis in Section 2.3 it follows that for a pipe which is several wavelengths long, the strain concentration at one end does not depend on the boundary condition at the other end. Similarly, the precise description of the excitation is not needed as it is only reflected by the amplitudes and phases of the incoming waves, one for each trigonometric order. Additionally, as the different waves travel with different speed, for broad band excitation they are on average uncorrelated. Thus, if the trigonometric orders are not coupled by the boundary conditions, on average they act independently at the boundary and the strain concentration does not largely depend on the excitation.

Considering this, the numerical experiments are made with a long pipe which is point excited at its middle and the total response for the trigonometric orders $n = 1$ to $n = 25$ is calculated. But for details in narrow bands, because of correlation between the waves, this experiment should be representative for any long pipe structure. The experiment depends only on the non dimensional numbers β, Ω and ν and on the boundary conditions at one end. By a systematic variation of these, the experiments presented below are a fairly complete study of the strain concentration in pipe structures.

4.1 INFINITE PIPE

An almost infinite pipe is investigated to give an idea of the strains within pipes. The pipe is 10^8 m long, the loss factors are $\eta_e = \eta_\nu = 10^{-5}$ while all other data are as given in Table 1. The maximum strain in a cross section 125 m away from the excitation and the rms average radial velocity in a 5 m long section are calculated.

The dynamic strain factor is shown in Figure 10. At low frequencies, when only the $n = 1$ beam mode is cut-on, Γ has a constant value $\Gamma \approx 2$. At the cut-on frequency of the $n = 2$ mode Γ increases by a factor $\sqrt{3\left(1+1/2^2\right)/2}$, as is explained in what follows.

At frequencies well below the ring frequency the average cross sectional kinetic energy density is to a good approximation given by equation (28)

$$e_k = RT_c \Lambda_n \rho \left(\omega w\right)^2 \left(1+1/n^2\right)/4.$$

Close to a modes cut-on frequency, the pipe response is dominated by this mode. Therefore, at the cut-on of the $n = 2$ mode, the ratio of the square root of the kinetic

energy to the radial velocity decreases by a factor $\sqrt{\left(1+1/2^2\right)/2}$, hence, the strain factor decreases this much. On the other hand, the strain energy in the $n = 1$ mode is entirely given by in-plane strain whereas at the cut-on of a higher order mode the strain energy is predominantly flexural [18]. With reference to equation (24), the strain factor therefore increases at cut-on by a factor $\sqrt{3}$. The combined effect of these two phenomena is that at cut-on of the $n = 2$ mode, $\Gamma \approx 2\sqrt{3\left(1+1/2^2\right)/2}$.

At a frequency $\sqrt{2}$ times the cut-on frequency, the strain energy becomes predominantly in-plane [22] so the strain factor decreases away from cut-on by a factor $\sqrt{3}$ compared to its maximum value at cut-on. At somewhat higher frequencies the vibrations are to a fair proportion given by both the $n = 1$ mode and the $n = 2$ mode, so the strain factor fluctuates and increases to an intermediate value for the two modes. This pattern repeats at the cut-on of the $n = 3$ and the $n = 4$ modes whereas at even higher frequencies the picture becomes less regular as the response is given by an increasing number of modes.

Despite the fluctuations discussed above, it is fair to draw the conclusion that within an infinite pipe the strain factor is limited in the range $1 < \Gamma < 4$. It is of the order $\Gamma \approx 2$ at low frequencies when only the $n = 1$ beam mode can propagate while, neglecting coherence effects, $\Gamma \leq 2\sqrt{3}$ at higher frequencies.

4.2 WITHIN A FINITE FLUID-FILLED PIPE

Within a finite pipe performing reverberant vibrations there is, for each trigonometric order that is cut-on, two waves (one in each direction) having approximately equal amplitudes. With two waves, instead of one wave, the rms velocity increases by a factor $\sqrt{2}$ while the maximum strain increases by a factor 2.

If in addition there is fluid within the pipe, for frequencies well below the cut-on of internal fluid modes, the cross sectional kinetic energy density is given by [18]

$$e_k = 2\pi R T_c \Lambda_n \rho \left(\omega w\right)^2 \left(1+1/n^2+2\mu/n\right)/4; \quad \mu = R\rho_f / 2T_c\rho. \tag{42}$$

This expression is a function of the trigonometric order n, while it is preferable to have it as a function of frequency. For frequencies where the $n \geq 2$ higher order modes dominates the response, the $1/n^2$ (tangential in-plane inertia) term is small while the combined radial and fluid inertia terms can be approximated [22]

$$1 + 2\mu/n \approx \left(1+2\mu\left(2\mu\Omega^2/\beta\right)^{-\frac{1}{5}}\right). \tag{43}$$

Combining this with the results in the previous section, it is found that the strain factor within a finite fluid-filled pipe, for uncorrelated trigonometric orders, is approximately given by

$$\Gamma \approx \begin{cases} 2\sqrt{2}\,(1+\mu), & f < f_{c2} \\ 2\sqrt{6}\left(1+2\mu\left(2\mu\,\Omega^2/\beta\right)^{-\frac{1}{5}}\right) & f > f_{c2} \end{cases} \tag{44}$$

where f_{c2} is the cut-on frequency for the $n = 2$ mode which is given by [22]

$$f_{cn} = \frac{c_L}{2\pi R}\sqrt{\beta\frac{n^2\left(n^2-1\right)^2}{1+n^2+2n\mu}}\ . \tag{45}$$

The strain factor estimate in equation (44) agrees with the measurements presented by Norton and Fahy [11].

4.3 Strain factor at the end of pipes

For pipes described with thin-walled cylinder theory, four boundary conditions are required at each end. In this paper, homogenous boundary conditions of the first and/or second kind are considered, that is, either the displacements or the force resultants are set to zero at the end. Thus the boundary conditions are [15]

$$\begin{array}{lll} u = 0 & \text{or} & N_x = 0, \\ v = 0 & \text{or} & S_{x\theta} = 0, \\ w = 0 & \text{or} & V_x = 0, \\ w_x = \partial w/\partial x = 0 & \text{or} & M_x = 0, \end{array} \tag{46}$$

where the explicit expressions for the force resultants $N_x, S_{x\theta}, V_x$ and M_x are given in [15, equation (2.144) and Tables 1.4 and 1.5]. However, they are not needed here since the spectral FE calculations are based upon a variational principle. Boundary conditions of the second kind are then natural boundary conditions, meaning that if no requirements are made on one of the displacement components, the boundary condition will automatically be that the corresponding force resultant is zero.

The boundary conditions are labelled as by Leissa [15, Section 2.4.6]. Thus, e.g., the blocked boundary condition is labelled (u, v, w, w_x) an the shear-diaphragm boundary condition is labelled (N_x, v, w, M_x).

A 200 m long pipe point excited at its middle is considered. The maximum strain at one end and the spatial rms average radial velocity in a section starting 1 m from the end and extending 5 m towards the source are calculated. The loss factors are $\eta_e = \eta_v = 10^{-6}$ at the pipe section where the strain is calculated and $\eta_e = \eta_v = 10^{-3}$ in the other section. Unless explicitly stated the other data are as specified in Table 1.

4.3.1. *Wall thickness*

To investigate the importance of the parameter β on the strain factor, three different wall-thickness' are considered: $R/T_c = 15$, $R/T_c = 40$ and $R/T_c = 120$. Calculations are made for the blocked boundary condition (u, v, w, w_x).

The calculated strain factors are plotted in Figure 11a in narrow band and in Figure 11b in third octave bands. Also shown in Figure 11b is the constant value $4\sqrt{2}$. As found in Section 3.3, at low frequencies the strain factor is constant. At cut-on of higher order modes, it first drops and then starts to fluctuates (because of coherence between different waves) and may become slightly larger. On average the strain factor $\Gamma = 4\sqrt{2}$ applies while in this experiment it is limited $\Gamma < 7$. It is concluded, but for details in narrow bands the strain factor does not depend on wall-thickness.

The factor $4\sqrt{2}$ is heuristically arrived at by arguing that the strain factor within a pipe is $2\sqrt{2}$. This value applies at anti nodes where the translational motion of the cross section is not restricted while the cross sectional rotation and the pipe wall rotation are zero. It then seems plausible that the strain doubles if also the former motions are restricted. This vague argumentation is justified by the results in Figure 11b.

4.3.2 *Poisons' ratio*

The strain factors dependence on Poisson's' ratio is investigated. The calculations are made, as in the previous section considering a blocked boundary, for pipes with wall-thickness $T_c = R/40$ and with Poisson's ratio: $\nu = 0$, $\nu = 0.3$ and $\nu = 0.5$. The results are for clarity shown in 1/3-octave bands in Figure 12. As can be seen, the strain factor drops approximately by 30 % for $\nu = 0$ while it is quite similar for $\nu = 0.3$ and $\nu = 0.5$. Concluding that the strain factor does not largely depend on Poisson's' ratio.

4.3.3 Other s*tandard boundary conditions*

For pipes, there are in total sixteen homogenous boundary conditions of the first and second kind. The blocked boundary condition (u, v, w, w_x) is discussed above. The other three standard boundary conditions are the free $(N_x, S_{x\theta}, V_x, M_x)$, the sliding $(u, S_{x\theta}, V_x, w_x)$ and the shear diaphragm (simply supported) (N_x, v, w_x, M_x) boundary conditions. The strain factors for the remaining twelve boundary conditions are presented in Section 4.4.. Most of them are not easily realised in practise so the engineering significance of this investigation is perhaps limited. However, the results raises some interesting questions.

Figure 13 shows the strain factors for three standard boundary conditions, for a pipe with $\nu = 0.3$ and $T_c = R/40$. The shear-diaphragm boundary condition (N_x, v, w, M_x) is special in that it does not introduce any near field components [15]. At frequencies below the ring frequency, the $n = 1$ waves in pipes are described with beam theory. For an Euler beam the strain is zero at a simply supported end. Similarly, for a Timoshenko beam the axial in-plane strain is zero but, increasingly with frequency, there is some in-

plane shear strain. Apparently, see Figure 13, this also applies for pipes. At the cut-on of higher order modes the dominating terms in the strain energy are the circumferential flexural and in-plane axial strains. Both these terms are zero at a shear diaphragm end and therefore the strain factor drops at cut-on. But for frequencies close to the ring frequency, the strain factor at a shear-diaphragm end is smaller than the one that applies within pipes.

The strain factor for a free boundary $(N_x, S_{x\theta}, V_x, M_x)$ is small at lower frequencies. At cut-on frequencies, where the circumferential flexural strain is large, the strain factor reaches the limiting value $\Gamma \approx 4\sqrt{2}$, the same that applies for a blocked boundary. Finally, the strain factor found for a sliding boundary $(u, S_{x\theta}, V_x, w_x)$ has a quite un-dramatic behaviour and is for all frequencies of the order of the one found within pipes.

In summary, the numerical experiments presented in this section show that, but for details in narrow bands the strain factor is independent of wall-thickness and it does not largely depend on Poisson's ratio. Additionally, if the maximum strain is sought regardless of whether it appears within the pipe or at its ends, the strain factor, within a factor of 2, is independent of both frequency and boundary condition. Thus, for the four boundary conditions considered, the calculated strain factors are in narrow bands limited $\Gamma < 7$ and on the average $\Gamma \leq 4\sqrt{2}$. For some boundary conditions, the strain factor has its maximum within the pipe.

4.4. OTHER BOUNDARY CONDITIONS

Above the strain factor for four "standard" boundary conditions were calculated. Figures 14 show the strain factor for the remaining twelve homogeneous boundary conditions of the first or second kind.

In Section 4.3.3. it was found that for the four boundary conditions considered the frequency averaged strain factor is limited: $\Gamma \leq 4\sqrt{2}$. In Section 2 it was argued that, since there is no reactive energy exchange at the end of a pipe where the boundary conditions are of the first or second kind, there should not be any local resonance's and therefore the amplitude of the near field terms should not be substantially greater than the amplitude of the incoming wave and, consequently, the strain factor should be limited. Apparently, see Figure 14, this is not true for all homogeneous boundary conditions; the strain factor calculated from the strain at the boundary is not limited to $\Gamma \leq 4\sqrt{2}$. However, when it is calculated from the strain 1 cm away from the boundary ($R/3 \approx 1\,cm$), it is for all sixteen boundary conditions limited.

For the boundary conditions (N_x, v, w, w_x), (N_x, v, V_x, w_x), $(N_x, S_{x\theta}, w, w_x)$ and $(N_x, S_{x\theta}, V_x, w_x)$ the strain factor increases at very low frequencies. All these boundary conditions have the rotation of the shell wall, w_x, restricted while the cross sectional rotation, u, is free. Figure 15 shows for the boundary condition (N_x, v, w, w_x) the strains for the $n = 1$ mode in the pipe at $\Omega = 1.26\,10^{-3}$ ($f = 10$ Hz) as functions of the distance from the boundary. Close to the boundary the axial strain is large while it decreases

exponentially at a rate corresponding to the real part of the standing decaying wave numbers ($\alpha = -248 \pm i245$ (1/m)).

For the boundary conditions $(u, S_{x\theta}, w, w_x)$, $(u, S_{x\theta}, w, M_x)$, $(N_x, S_{x\theta}, w, w_x)$ and $(N_x, S_{x\theta}, w, M_x)$ the strain factor increases at intermediate frequencies. These boundary conditions have the radial but not the tangential displacement blocked. In Figure 16 are plotted the strain factors for the trigonometric orders 1 to 12 for the boundary condition $(u, S_{x\theta}, w, M_x)$ showing that the large strain factor found in Figure 14b is predominantly due to the $n = 1$ mode.

Using beam theory for describing the $n = 1$ pipe vibrations, the restraints on motion are that the tangential and radial displacements are proportional and that, at low frequencies, the cross sectional rotation is proportional to the slope of the radial displacement, i.e., to the shell wall rotation. The two groups of boundary conditions considered above do not fulfil both these restraints, so, the standing decaying waves are excited. This is verified by inspecting the relative amplitudes of the waves at the boundary showing that the standing decaying near field waves have a large amplitude when the strain factor is large. In Figure 15, it is notable, at a distance away from the boundary equal to the wall thickness (0.82 *mm*) the axial strain has decreased by 20 %. This rapid decrease makes the application of thin-walled shell theory not entirely satisfactory. However, it is beyond the scope of the present work to doubt such theory.

In conclusion, for most boundary conditions the strain factor is limited $\Gamma \leq 4\sqrt{2}$. However, for some boundary conditions that are in conflict with the restrains on motion imposed by beam theory, the strain factor is larger than this. In these cases there is a large concentration of strain decaying exponentially away from the boundary. The rate of decay is so rapid that it would be difficult to measure it and as it seems difficult to find a practical situation where these boundary conditions are applied, the engineering significance of the finding of the large strain concentration is perhaps limited.

4.5 AXI-SYMMETRIC MODES

At frequencies below the ring frequency there are two $n = 0$ axi-symmetric modes that can propagate, the in-plane longitudinal mode and the torsional mode. The $n = 0$ longitudinal mode is included in the analysis in Section 3 but, as its mobility is low for radial excitation, it does not much influence the results.

Both axisymmetric modes have different relations between radial velocity and kinetic energy than the one given in equation (28) which applies for the $n \geq 1$ radial-axial modes. The torsional mode has, using thin-walled cylinder theory, no radial motion. Thus, per definition, the strain factor defined in equation (30) is infinite for this mode. Similarly, there is some radial motion, because of 'Poisson coupling' in the longitudinal mode, however, the strain factors would be very large if equation (30) were applied. So the velocity method can not be used to detect strain associated with the axi-symmetric modes if it is based on only radial accelerometer measurements.

An alternative would instead be to apply the velocity method with three-axial accelerometers estimating the total kinetic energy. The in-plane kinetic energy is low for the higher order radial-axial modes while it is approximately equal to the one for radial motion for the $n = 1$ mode. Thus, estimating the strain from the total kinetic energy should not much alter the results found in the previous sections.

Considering this, when large in-plane motion is expected the strain factor should be

$$\Gamma = (\gamma)_{\max} \frac{c_L}{V}; \quad c_L = \sqrt{E/\rho}; \quad V = \sqrt{\langle \omega^2 (u^2 + v^2 + w^2) \rangle}. \tag{47}$$

To investigate this idea the strain factor, equation (47), is calculated for a pipe with $\nu = 0.3$ and $T_c = R/40$. A blocked boundary is considered and in turns the pipe is excited with a radial, axial and transverse point force in its middle. Figure 17 shows the strain factors calculated when only the $n = 0$ modes are considered. At low frequencies the strain factors are large as the section where the kinetic energy is calculated is smaller than the wavelength so, because of the blocked boundary condition, the averaged kinetic energy in the pipe is underestimated. The strain factors for axial and radial excitations are identical, both these forces exciting the longitudinal but not the torsional mode. Besides at low frequencies, it has the almost constant value of $\Gamma \approx 2$, the same result as that which follows from Hunts analysis for rods [7]. The transverse force excites only the torsional mode and results in a strain factor $\Gamma \approx 2\, c_T / c_L = 2\sqrt{G/E}$.

Figure 18 shows the strain factors calculated for the three force excitations considering all the trigonometric orders 0 to 16. It is seen that the strain factors drop somewhat as compared to the results in Section 4.3. At low frequencies, when only the $n = 1$ beam mode and the $n = 0$ axi-symmetric modes can propagate, the strain factor based on equation (47) is approximately $\Gamma \approx 4$. At somewhat higher frequencies, when the $n \geq 2$ radial-axial modes can propagate, it increases to be approximately $\Gamma \approx 4\sqrt{2/(1+1/n^2)}$. Finally, for frequencies close to the ring frequency the restraints against in-plane motion decreases and the strain factor drops somewhat.

In conclusion, when the axi-symmetric $n = 0$ modes are excited, the velocity method for estimating dynamic strain must be based on the total kinetic energy as in equation (47). In this case the strain factor will be dependent on which of the modes that dominates the response and thus it will be dependent on the excitation. It is $\Gamma \approx 1.2$ for torsional modes, $\Gamma \approx 2$ for longitudinal modes, $\Gamma \approx 4$ for beam modes and finally it reaches $\Gamma \approx 6$ for higher order radial-axial modes. This range of values means that, without precise knowledge of the vibration field, it is difficult to predict fatigue life with the velocity method. However, it should still be very useful for assessing fatigue risk.

5. CONCLUSIONS

The velocity method for estimating strain in pipe structures is investigated. With this method predicted or measured spatial rms vibration velocity and theoretically derived strain factors are used to estimate maximum strain. Therefore, results from SEA can be used for estimating strain. When measuring strain, it is not practical to instrument large pipe works with strain gauges 'everywhere' while it may be possible to perform vibration measurement using portable equipment. Thus, the method facilitates assessments of fatigue

Theoretical investigations are made showing that the strain in a point is limited by an expression proportional to the strain energy density which in turn is related to its cross sectional average. For reverberant field or for infinite pipes, the average strain energy density is equal to the average kinetic energy density. For the radial-axial modes of order $n \geq 1$ the square root of the kinetic energy density is proportional to the radial vibration velocity. It is argued that the strain at a pipe end should be proportional to the amplitudes of the incoming vibrational waves and thus to the average strain energy density. Upon this basis, the non-dimensional 'strain factor' Γ is defined as the maximum strain times the ratio of the sound velocity in the pipe material to the rms averaged radial vibration velocity. Measurements and numerical experiments are made to investigate whether the strain factor is an effective and descriptive non-dimensional number.

Measurements made at the blocked end of a plastic pipe show that the strain factor is an almost constant function of frequency with a value of the order of those previously reported [11 14]. The strain measurements are made with piezo electric film gauges that has a high sensitivity and a good linearity [20, 21]. The measurements are compared to calculations using the spectral finite element method presented in [4], here developed by routines for calculating average vibration response and for calculating strain and stress. The results agree very well, this justifying numerical simulations of the strain concentration in pipes.

Pipe vibration is a function of only four non-dimensional numbers, the excitation and the boundary conditions. For long pipes, the strain at one end depends only on the boundary conditions at the other end and on the excitation via the amplitudes of the relatively few incoming waves. If the excitation is of random and broadband character, the incoming waves are uncorrelated. Then the strain factor can be calculated without considering the excitation and the boundary conditions at the other end in detail. Considering this, numerical experiments are made on a long pipe excited by a point force at its middle. A deterministic point force is used for convenience but also as it provides a check on the sensitivity of the results on the assumption of uncorrelated excitations.

The four non-dimensional numbers n, ν, β and Ω and the boundary conditions are all varied. It is found that for blocked boundary conditions the trigonometric order, Poissons' ratio, wall-thickness and frequency only have a limited influence on the strain factor. All possible homogenous boundary conditions of the first and second kind, sixteen in all, are considered. For most of these boundary conditions the strain factors are limited by the value for the blocked boundary condition: $\Gamma \approx 6$. For some of the

boundary conditions the largest strain is found within the pipe; the strain factor is then reduced by approximately a factor of two.

The $n = 0$ axi-symmetric modes have no or little radial motion so, when these modes are excited, the velocity method has to be based on the total kinetic energy density including the in-plane motion. This can be accomplished with three-axial accelerometer measurements. Numerical experiments are made showing that the velocity method, based on total rms vibration amplitude, can be used to simultaneously detect the maximum strain for both in-plane and out-of-plane modes. However, the calculated strain factors depend on which modes that are excited, ranging from $\Gamma \approx 1.2$, for the torsional mode, to $\Gamma \approx 6$, for higher order radial-axial modes. This range of values means that it is difficult to predict fatigue life with the velocity method. However, it should still be very useful for assessing fatigue risk.

For two groups of boundary conditions the strain factors exceed the one for the blocked boundary. The large strain factors are found for the $n = 1$ beam mode when the boundary conditions are in conflict with the restraints on motion imposed by beam theory. These restraints are that the tangential displacement is proportional to the radial displacement and, at low frequencies when Euler beam theory is valid, that the cross sectional rotation (axial displacement divided by the radius) is equal to the shell wall rotation (the slope of the radial displacement). Beam theory describes the waves within pipes with high accuracy when compared to shell theory [18]. Thus, if the restraints on motion put up by beam theory are in conflict with the additional boundary conditions required by shell theory, the additional waves that are found for shells are excited. These solutions are 'standing decaying waves' with high wavenumbers, i.e., rapidly decaying oscillating functions. This reasoning has been confirmed with numerical experiments where high strain concentrations, caused by standing decaying waves, have been found when the boundary conditions are that the tangential displacement is free while the radial displacement is blocked. High strain concentrations are also found for low frequencies if the axial displacement is free and the rotation of the shell wall is blocked.

The boundary conditions discussed above are rarely found in pipe works. Thus, the existence of large strain factors does not much restrict the practicality of the velocity method for finding maximum strain at the end of pipes. However, pipes often fail at small bore connections and at unsupported masses, e.g., at T-junctions, flanges, pressure gauges and valves. Such connections may well introduce conditions on motion that are similar to those that applies for the boundary conditions discussed, this possibly resulting in high strain concentrations. Indeed, for flanges, at the frequency of total transmission, large vibrations including standing decaying waves have been found [23]. Also for a straight pipe with a discrete mass, large vibration amplifications were found at the cut-on frequencies of higher order radial-axial modes [4]. Consequently, before the velocity method can be used with confidence, more research in this area has to be undertaken to find limits for the strain concentration at equipment mounted on pipes.

ACKNOWLEDGEMENT

This work was financially supported by EPSRC, UK. The first authors three year repose at the ISVR was assisted by grants from TFR, Sweden.

REFERENCES

1. M. El-Raheb and P. Wagner 1985 *Journal of the Acoustical Society of America* **78**, 738-746. Harmonic response of cylindrical and toroidal shells to an internal acoustic field. Part 1: Theory

2. A. Wang and R. J. Pinnington 1990 *Proc. Inst. of Acoustics* **12** 477-484. An impedance approach to pipework analysis using the transmission matrix method.

3. C. de Jong 1994 *Ph. D. Thesis Technisce Universiteit Eindhoven.* Analysis of pulsations and vibrations in fluid-filled pipe systems

4. S. Finnveden 1997 *Journal of Sound and Vibration* **199**, 125-154 Spectral finite element analysis of the vibration of straight fluid-filled pipes with flanges.

5. M. P. Norton and A. Pruiti 1991 *Applied Acoustics* **33**, 313-336. Universal prediction schemes for estimating flow-induced industrial pipeline noise and vibration.

6. S. Finnveden 1997 *Proc. of the IUTAM symposium on Statistical Energy Analysis, Southampton.* Statistical energy analysis of fluid-filled pipes. (To be published by Kluwer academic publishers.)

7. F. V. Hunt 1961 *Journal of the Acoustical Society of America* **33**, 633-639.

8. E. E. Ungar 1961 *Journal of the Acoustical Society of America* **33**, 633-639. Transmission of plate flexural waves through reinforcing beams; dynamic stress concentrations.

9. S. M. Stearn 1970 *Journal of Sound and Vibration* **12**, 85-97. Spatial variation of stress, strain and acceleration in structures subject to broad frequency band excitation.

10. S. M. Stearn 1971 *Journal of Sound and Vibration* **15**, 353-365. The concentration of dynamic stress in a plate at a sharp change of section.

11. M. P. Norton, F. J. Fahy 1988 *Noise Control Engineering Journal* **30**, 107-117. Experiments on the correlation of dynamic stress and strain with pipe wall vibrations for statistical energy analysis applications.

12. L. L. Koss and D. Karzub 1995 *Journal of Sound and Vibration* **184**, 229-244. Euler beam bending wave solution predictions of dynamic strain using frequency response functions.

13. D. Karzub 1996 *Ph. D. Thesis, The University of Western Australia.* The prediction of dynamic stress and strain in randomly vibrating structures using velocity measurements.

14. D. Karzub and M. P. Norton 1997 *Proc. of the IUTAM Symposium on Statistical Energy Analysis, Southampton.* The estimation of dynamic stress and strain in beams, plates and shells using strain-velocity relationships. (To be published by Kluwer academic publishers.)

15. A. W. Leissa 1973 *NASA* **SP-288**. Vibrations of Shells. Washington DC: U.S. Gov. Printing Office.

16. R. N. Arnold and G. B. Warburton 1949 *Proc. Royal Soc. London, series A* **197**, 238-256. Flexural vibrations of the walls of thin cylindrical shells having freely supported ends.

17. Y. C. Fung 1965 *Foundations of Solid Mechanics*. Prentice-Hall.

18. S. Finnveden 1997 *Journal of Sound and Vibration* **208**, 685-703. Simplified equations of motion for the radial-axial vibrations of fluid filled pipes.

19. R. S. Langley 1994 *Journal of Sound and Vibration* **169**, 29-42. Wave motion and energy flow in cylindrical shells.

20. S. H. Liu and R. J. Pinnington 1996 *Proc. Inter Noise*, 2773-2776. Measurement of flexural and longitudinal wave power flow in beams with piezoelectric films.

21. S. H. Liu 1996 *Ph D. Thesis University of Southampton.*

22. S. Finnveden 1997 *Journal of Sound and Vibration* **208**, 705-728. Formulas for modal density and for input power from mechanical and fluid point-sources in fluid-filled pipes.

23. S. Finnveden 1997 *Proc. Sixth International Conference on Recent Advances in Structural Dynamics, Southampton* 613-627. Vibration energy transmission in fluid-filled pipes connected with flanges.

Table 1 *Pipe data*

$E \ (N/m^2)$	$\rho \ (kg/m^3)$	ν	$R \ (mm)$	$T_c \ (mm)$
$3.55\ 10^9$	$1.43\ 10^3$	0.4	33	1.9

η_e	η_v
0.025	0.01

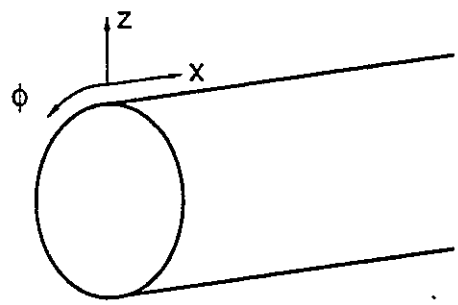

Figure 1. Cylinder coordinate system.

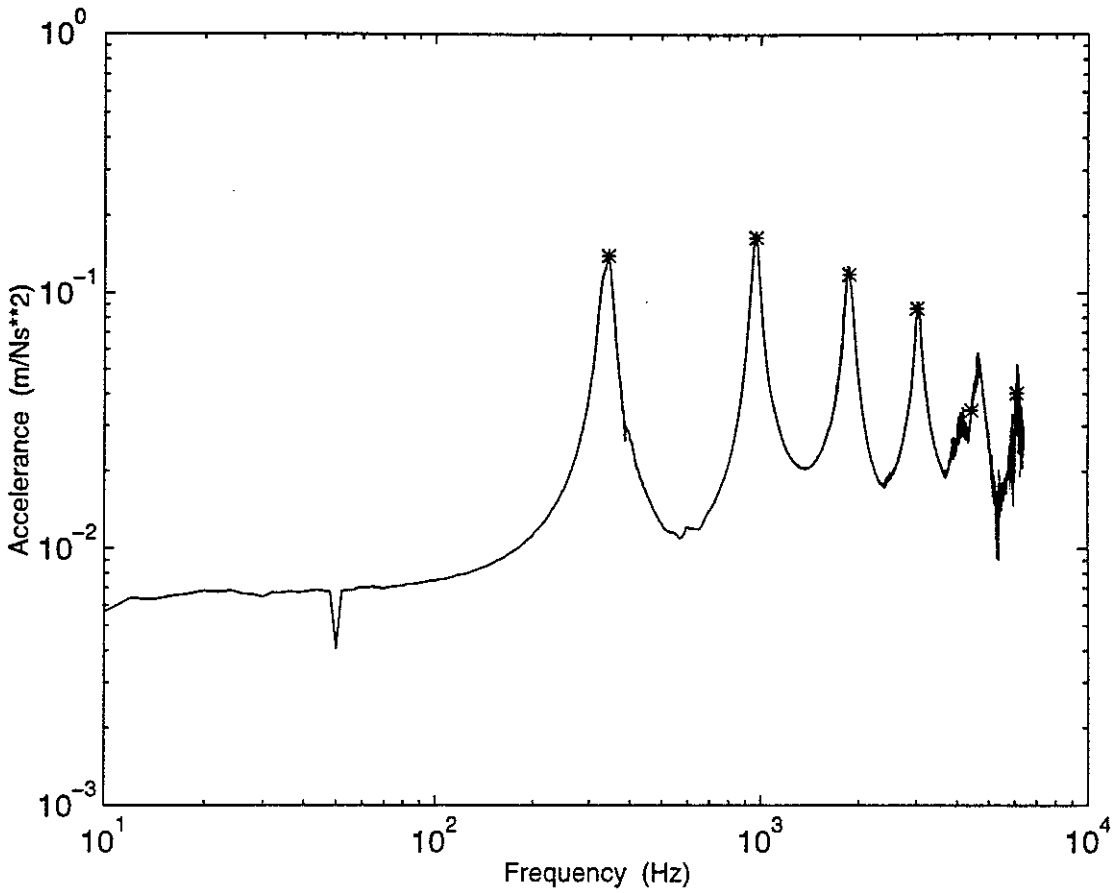

Figure 2. Accelerance of ring cut from plastic pipe. '*', cut-on frequencies, equation (31), with Young's modulus obtained from a curve fit.

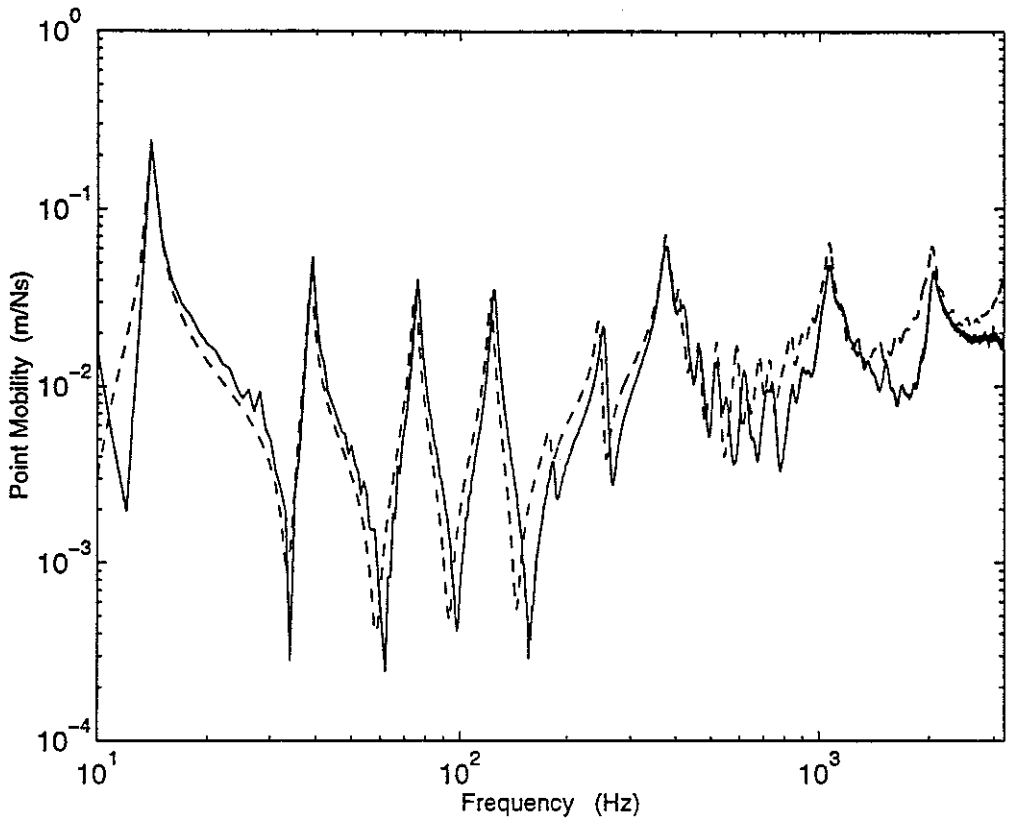

Figure 3. Point mobility of plastic pipe; '——', measured; '– – –', calculated.

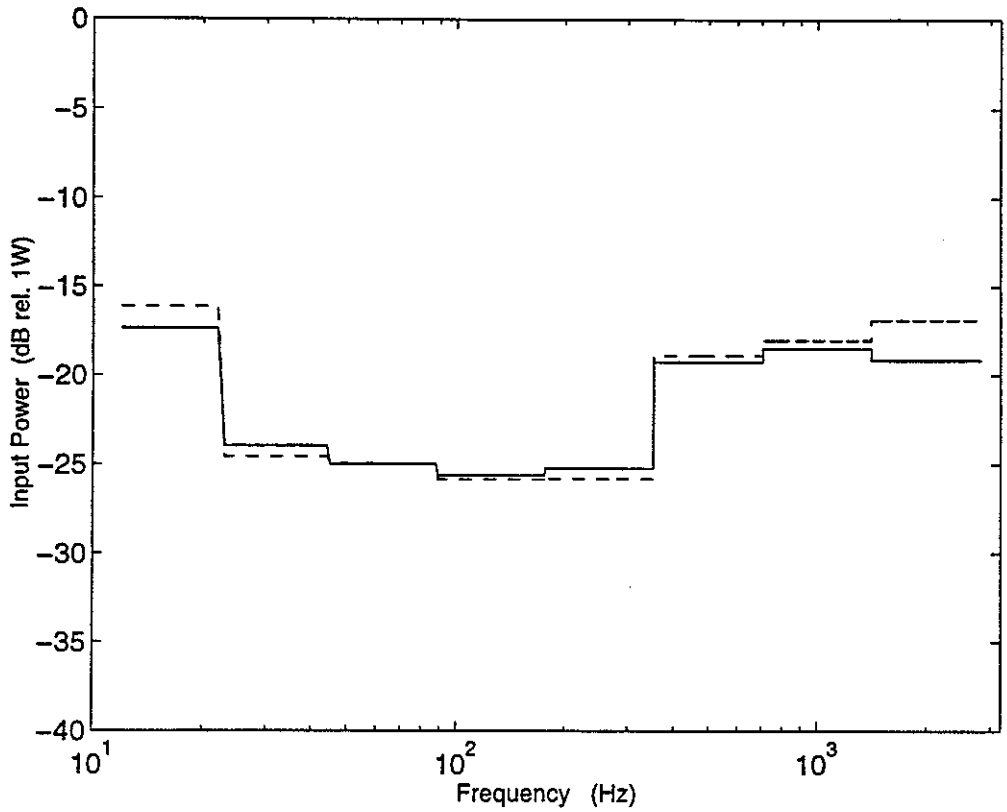

Figure 4. Octave band averaged Input Power to plastic pipe; '——', measured; '– – –', calculated.

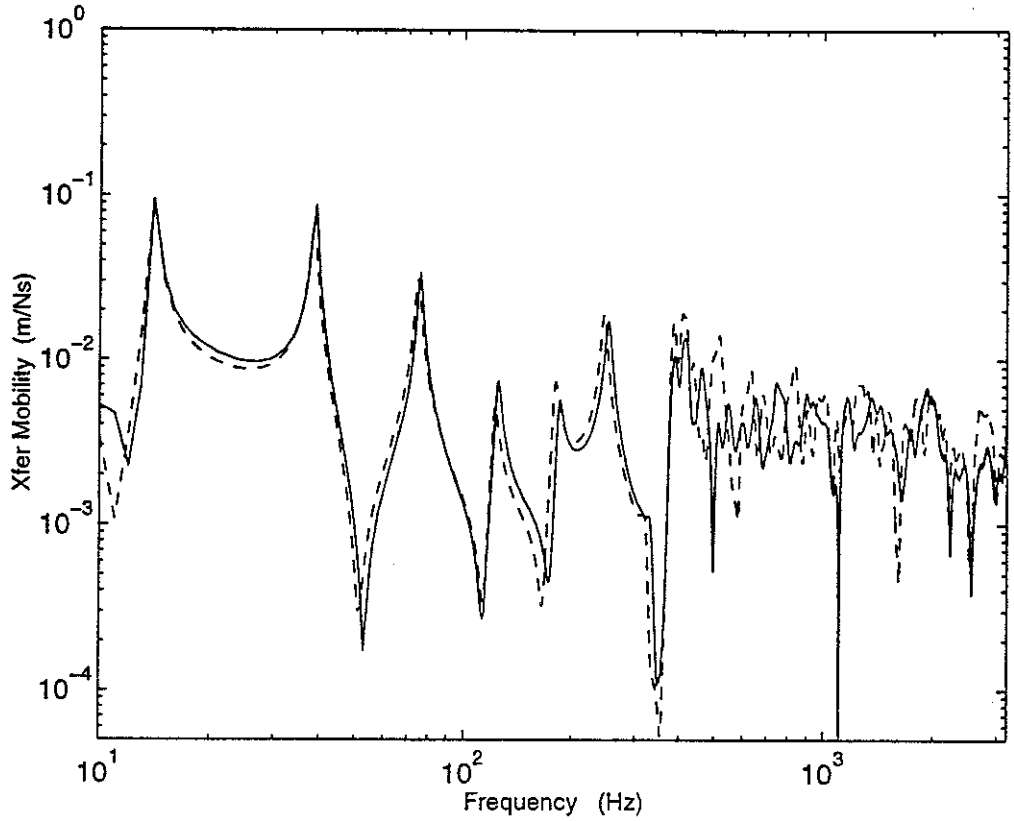

Figure 5. Transfer mobility in plastic pipe; '——', measured; '– – –', calculated.

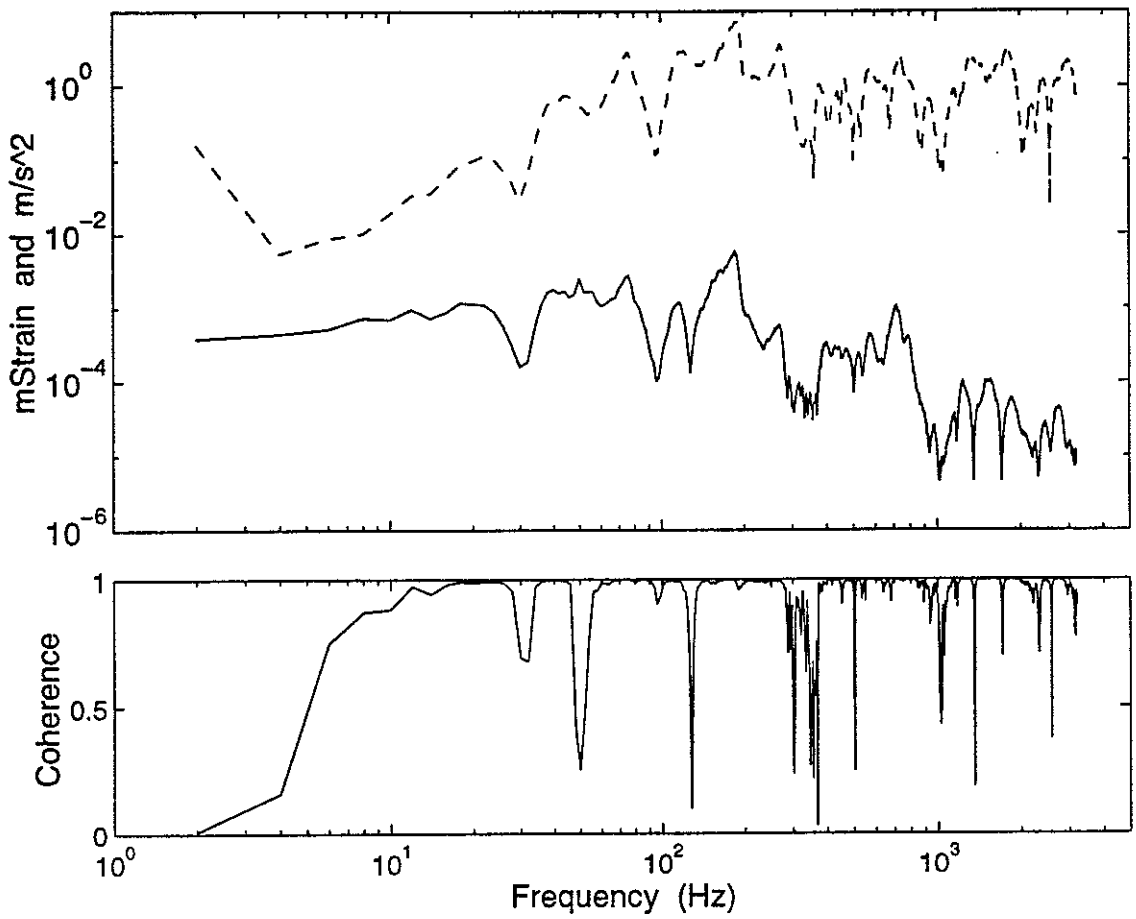

Figure 6. Upper, '——', Strain at point 1 (in milli strain); '– – –', acceleration of one accelerometer (m / s^2); Lower, Coherence.

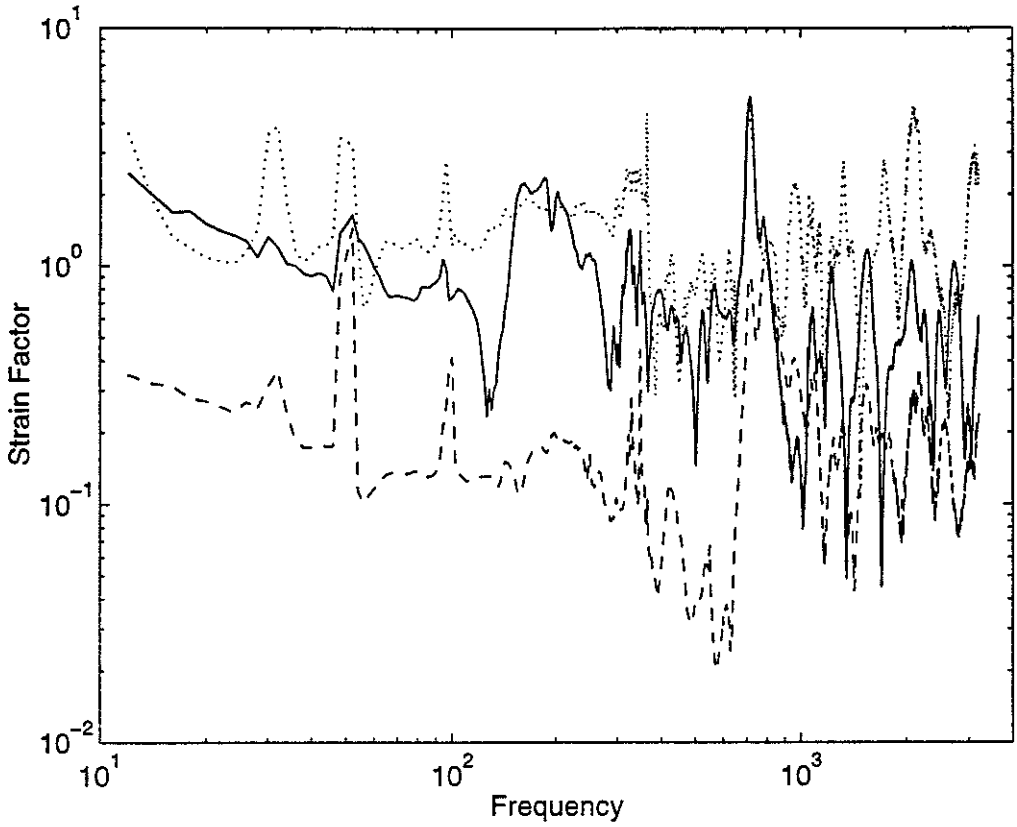

Figure 7a. Axial strain at blocked end of pipe times sound velocity in pipe material divided by rms radial vibration velocity. '——', Point 1; '– – –', Point 2; '• • • •', Point 3.

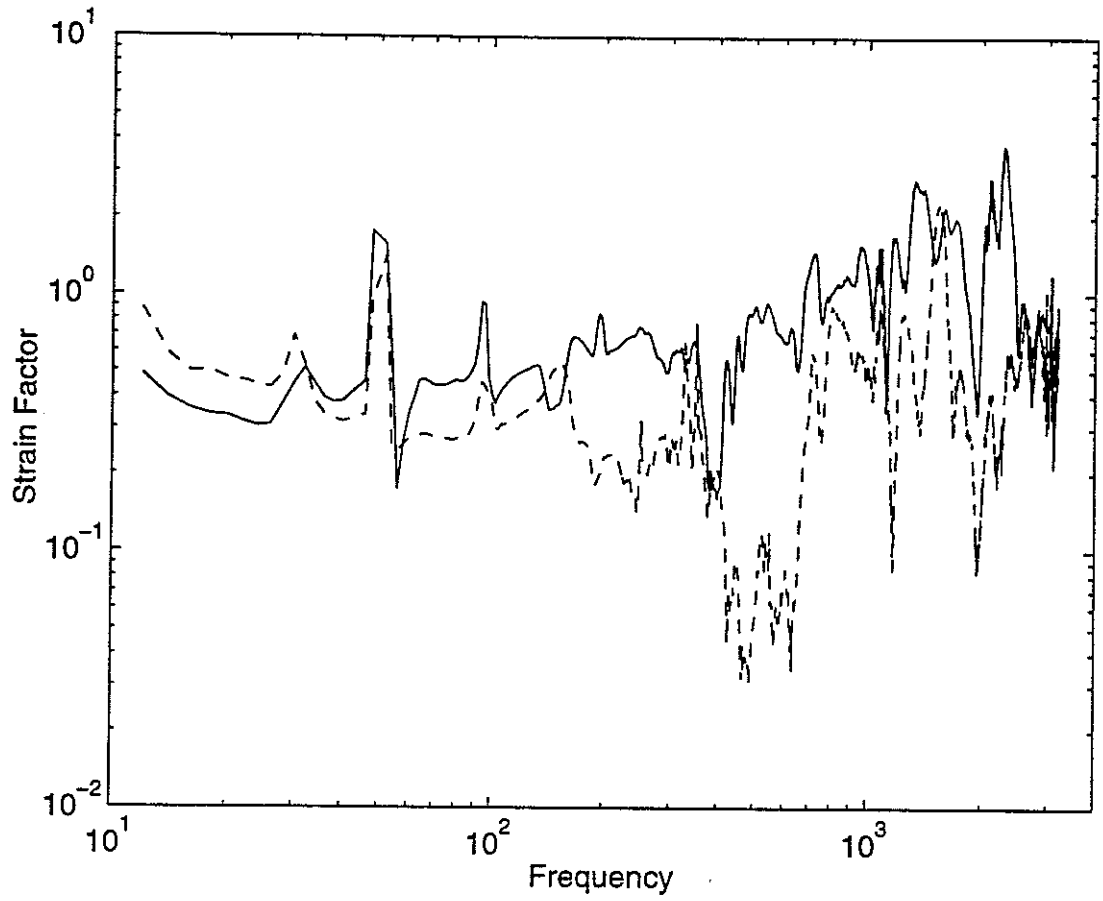

Figure 7b. Circumferential strain at blocked end of pipe times sound velocity in pipe material divided by rms radial vibration velocity. '——', Point 4; '– – –', Point 5;

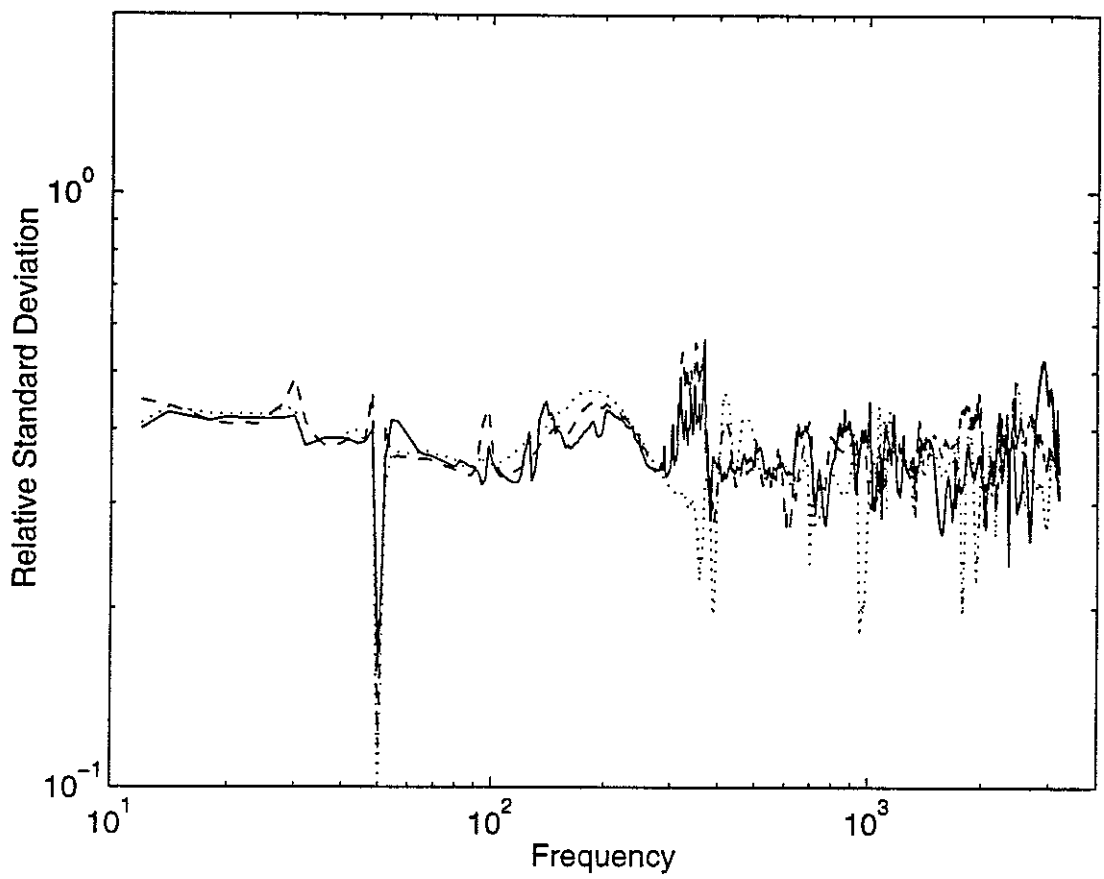

Figure 8. Relative standard deviation of estimated value of rms radial vibration velocity. Legends as in 7a.

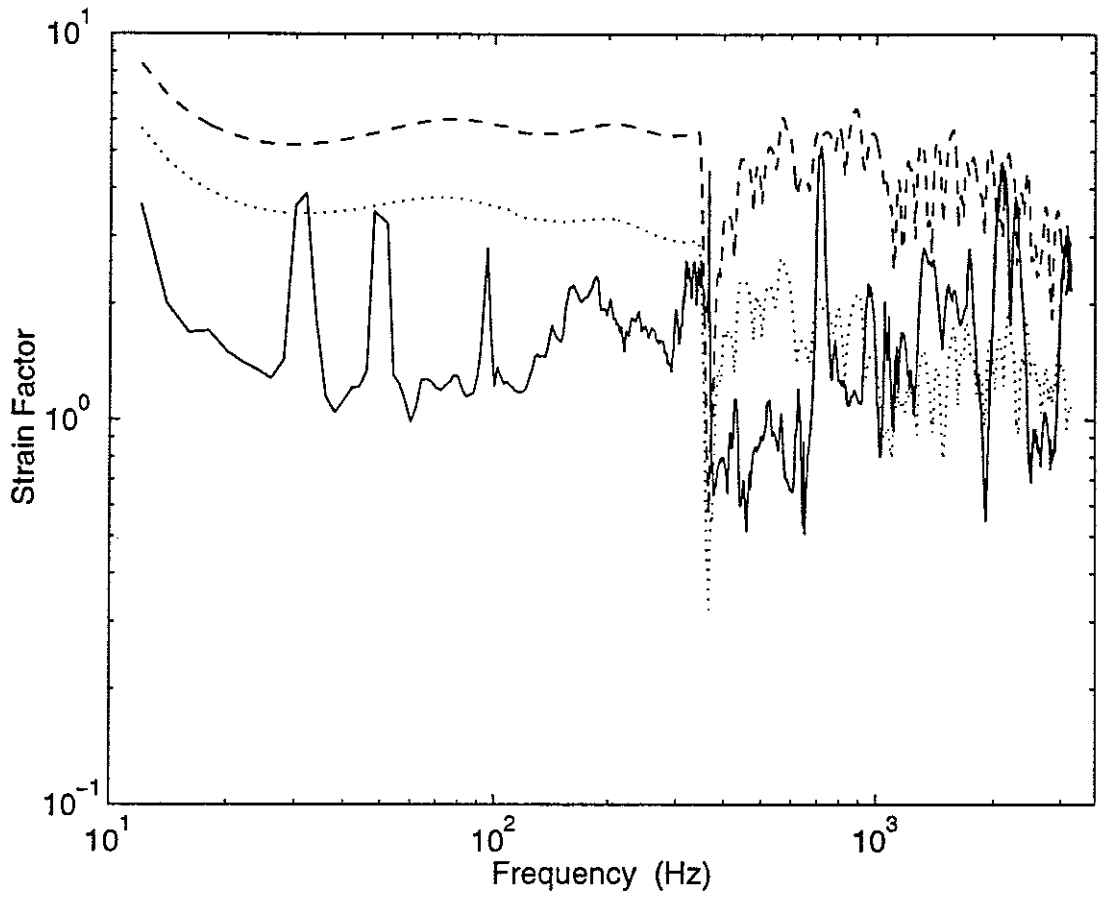

Figure 9. Maximum strain at blocked end of pipe times sound velocity in pipe material divided by rms radial vibration velocity. '——', estimated from five strain measurements; '– – –', calculated. ; '· · · ·', calculated in a point 2 *cm* from the end.

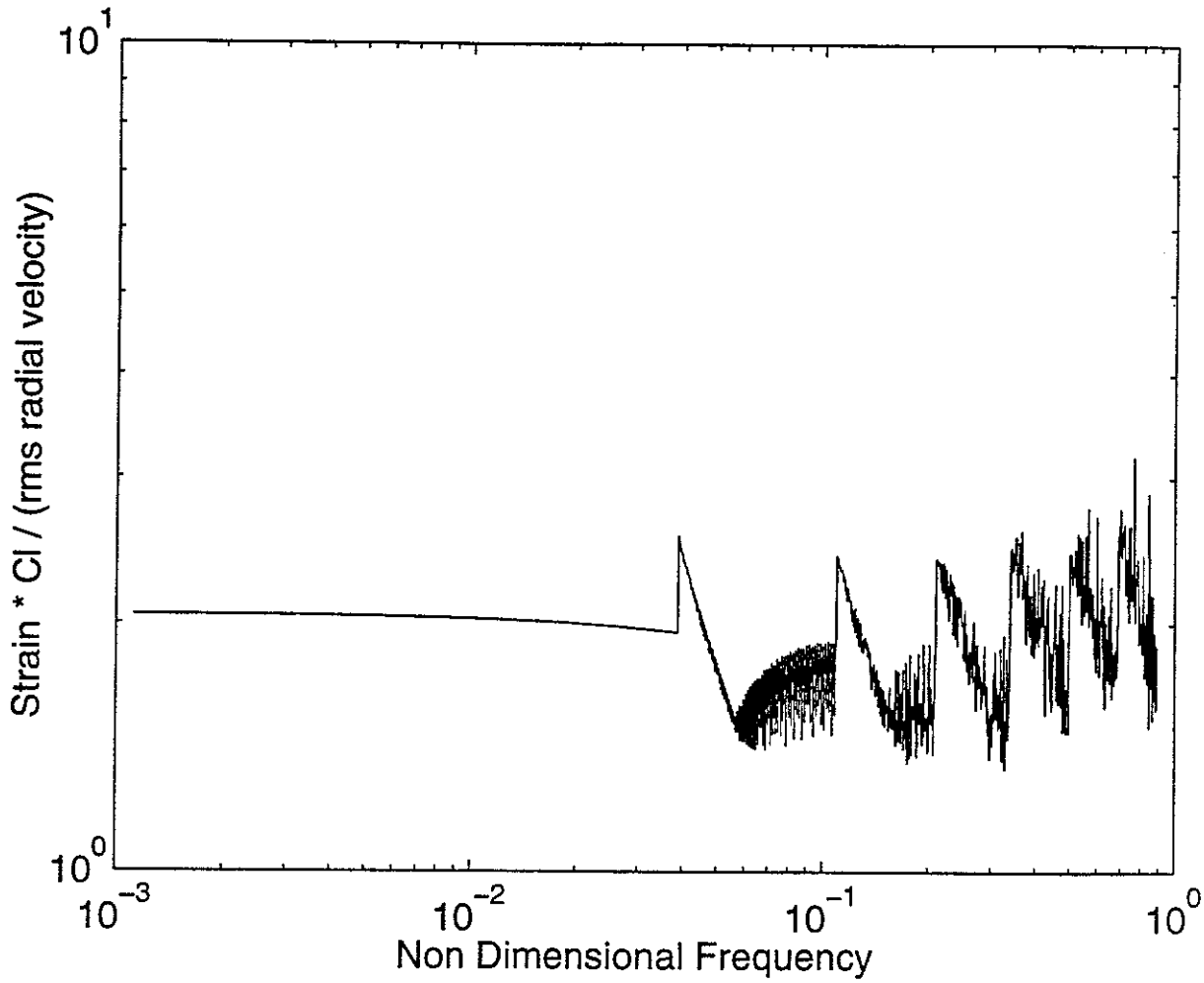

Figure 10. Strain factor in an infinite pipe.

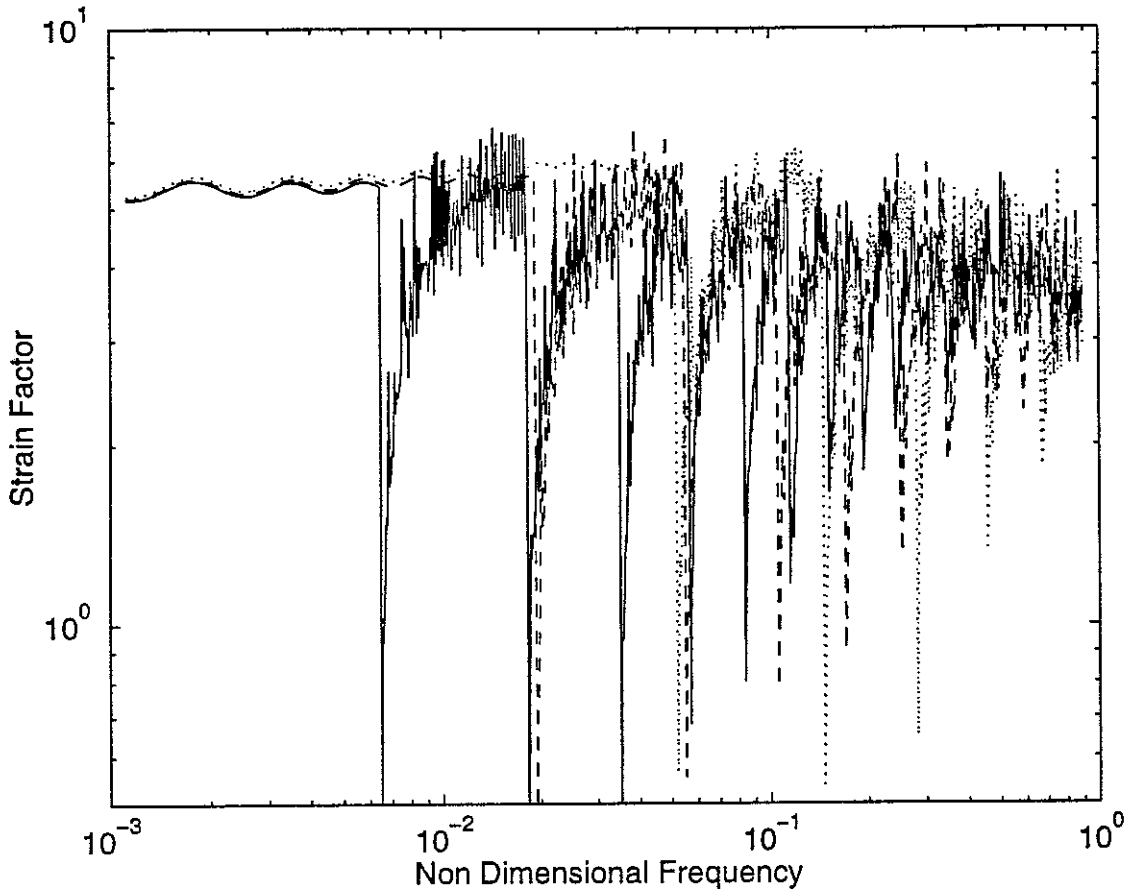

Figure 11a. Strain factor at blocked end. ——, $T_c = R/120$; – – –, $T_c = R/40$; ·····, $T_c = R/15$;

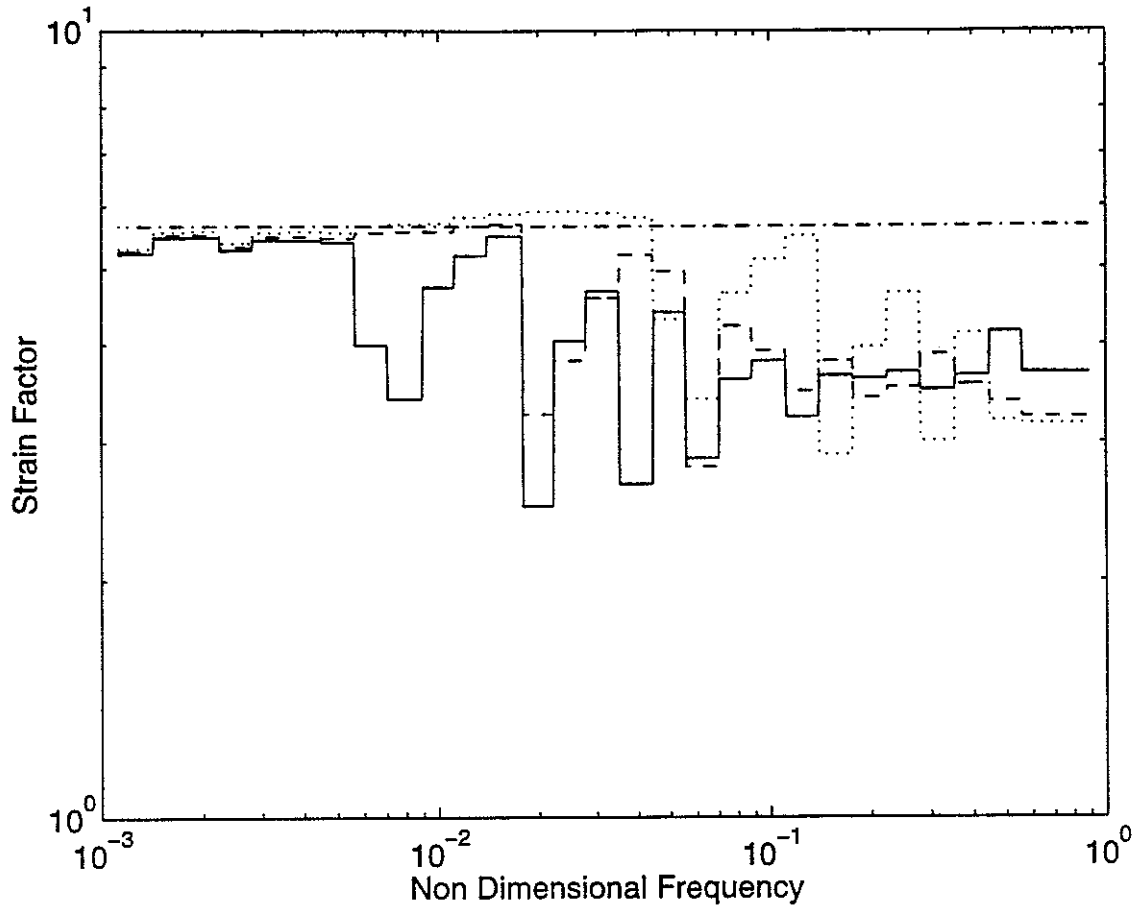

Figure 11b. Strain Factor at blocked end in one third octave bands.
——, $T_c = R/120$; – – –, $T_c = R/40$; ·····, $T_c = R/15$; –·–·, $4\sqrt{2}$.

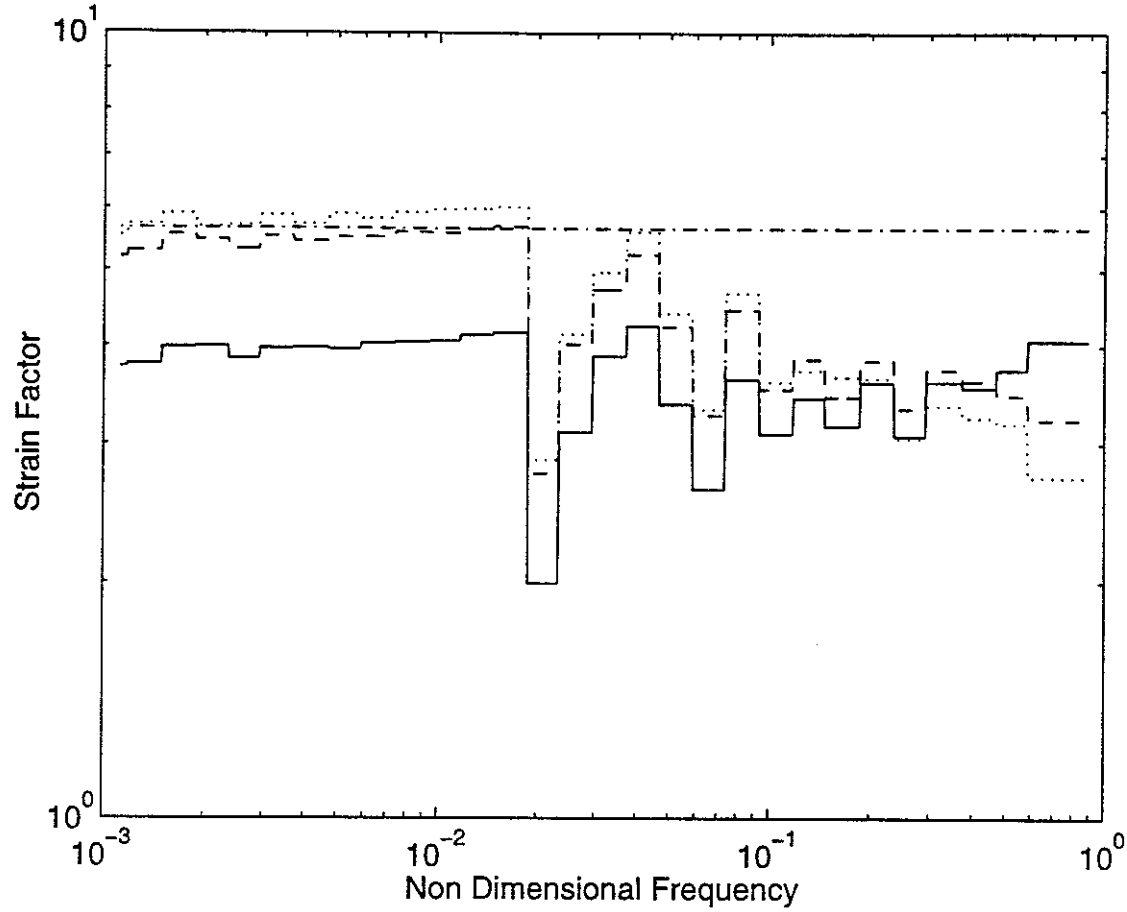

Figure 12. Strain Factor at blocked end in one third octave bands. ——, $\nu = 0$; – – –, $\nu = 0.3$; ·····, $\nu = 0.5$; –·–·, $4\sqrt{2}$.

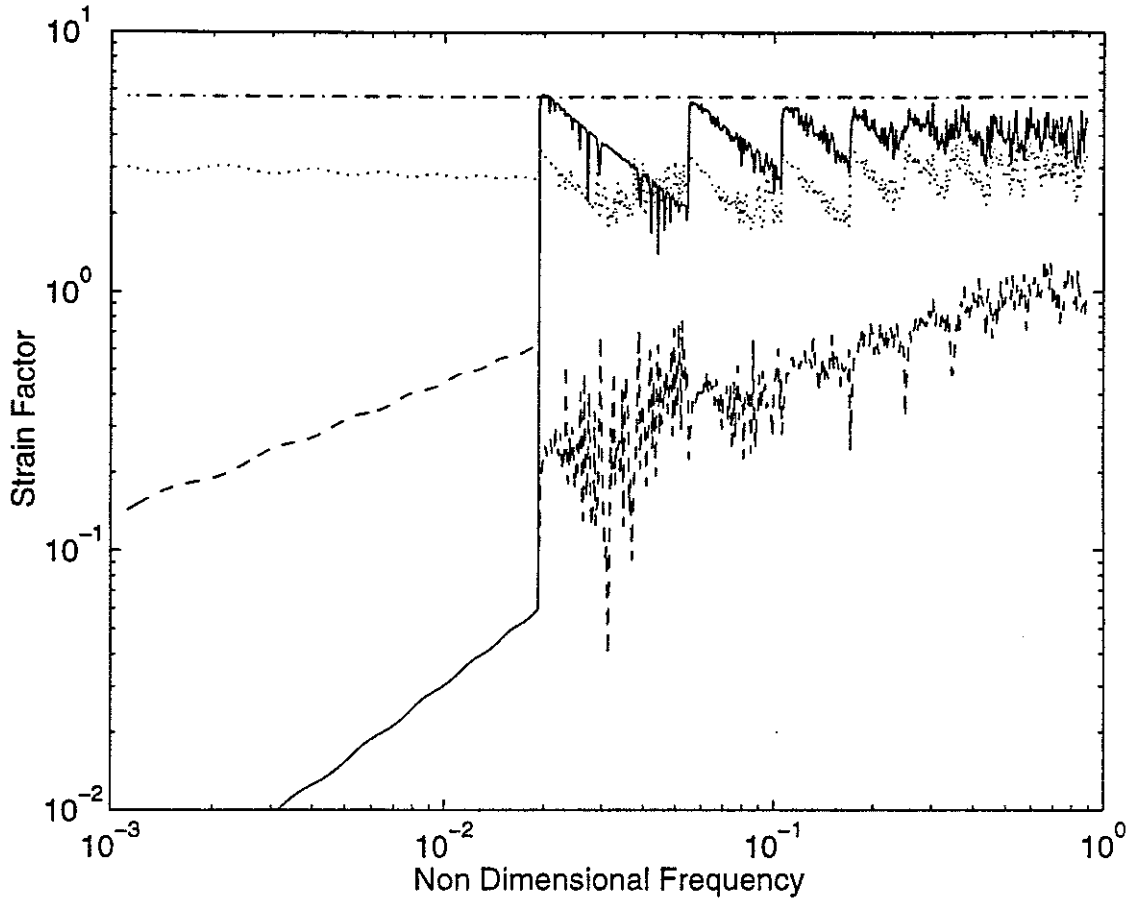

Figure 13. Strain factor. ——, at Free end; – – –, at Shear-Diaphragm end; ·····, at Sliding end; –·–·, $4\sqrt{2}$.

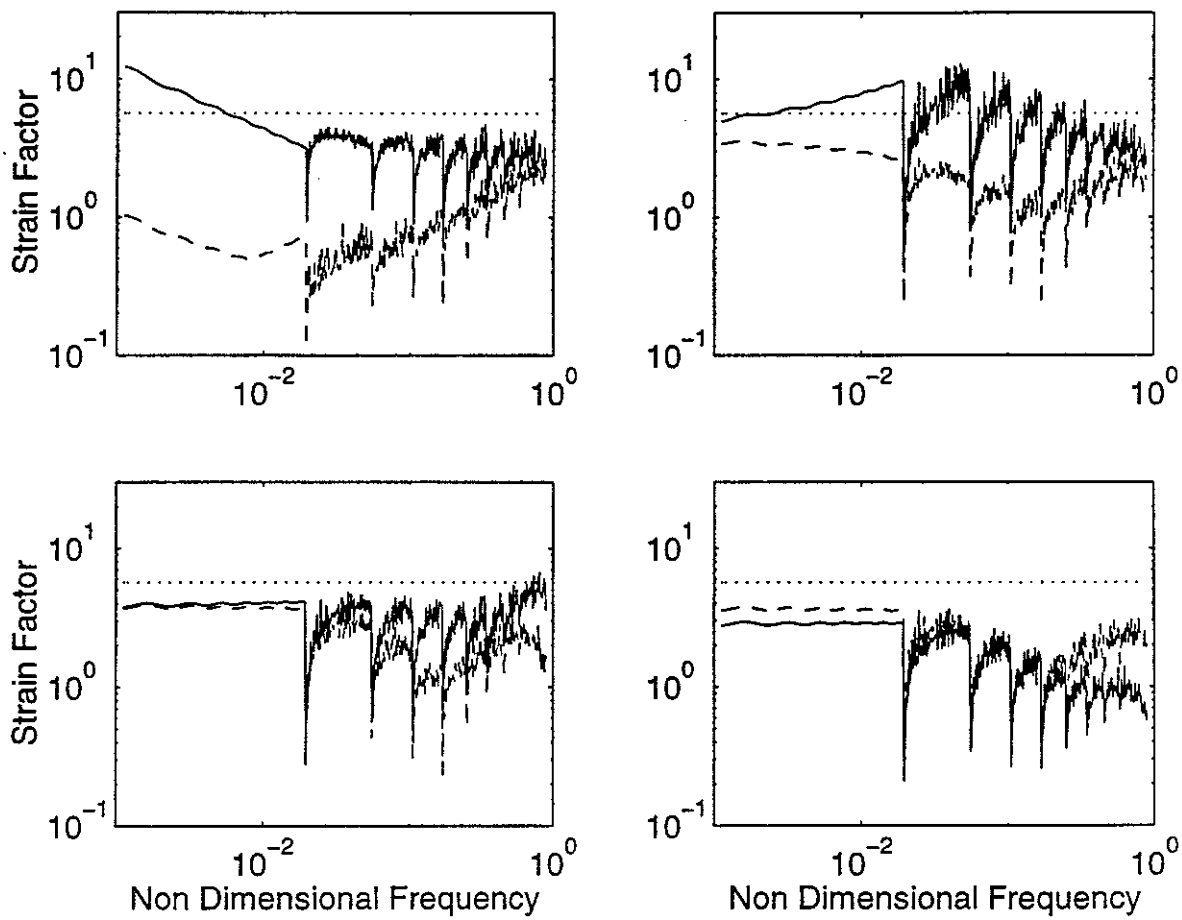

Figure 14 a. Strain Factor for different boundary conditions, $R/T_c = 40$, $\nu = 0.3$, ——, at end; – – –, 1 cm from end; ····; $4\sqrt{2}$; (a), (N_x, v, w, w_x); (b), $(u, S_{x\theta}, w, w_x)$; (c), (u, v, V_x, w_x); (d) (u, v, w, M_x).

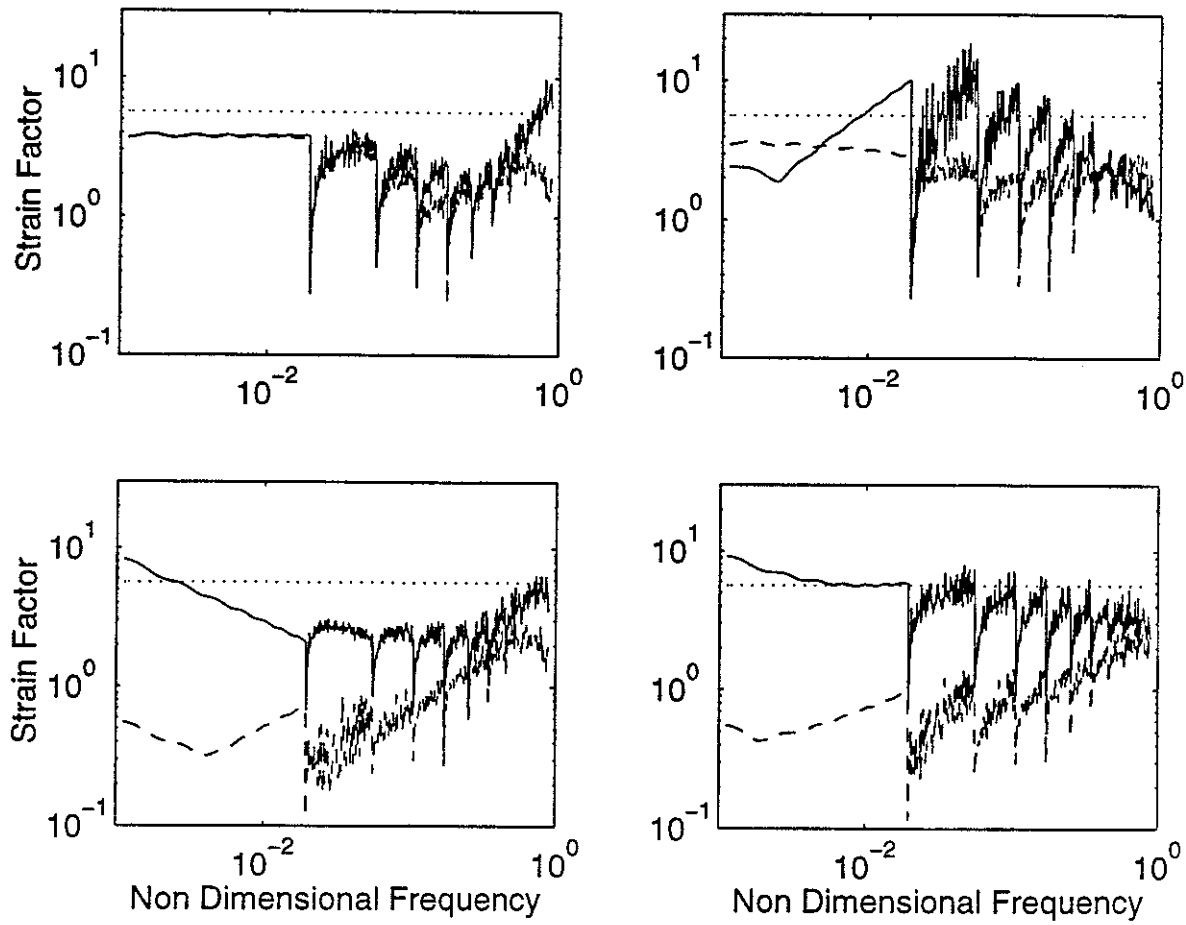

Figure 14 b. Strain Factor for different boundary conditions, $R/T_c = 40$, $\nu = 0.3$; ——, at end; – – –, 1 cm from end; ····; $4\sqrt{2}$; (a), (u, v, V_x, M_x); (b), $(u, S_{x\theta}, w, M_x)$; (c), (N_x, v, V_x, w_x); (d) $(N_x, S_{x\theta}, w, w_x)$.

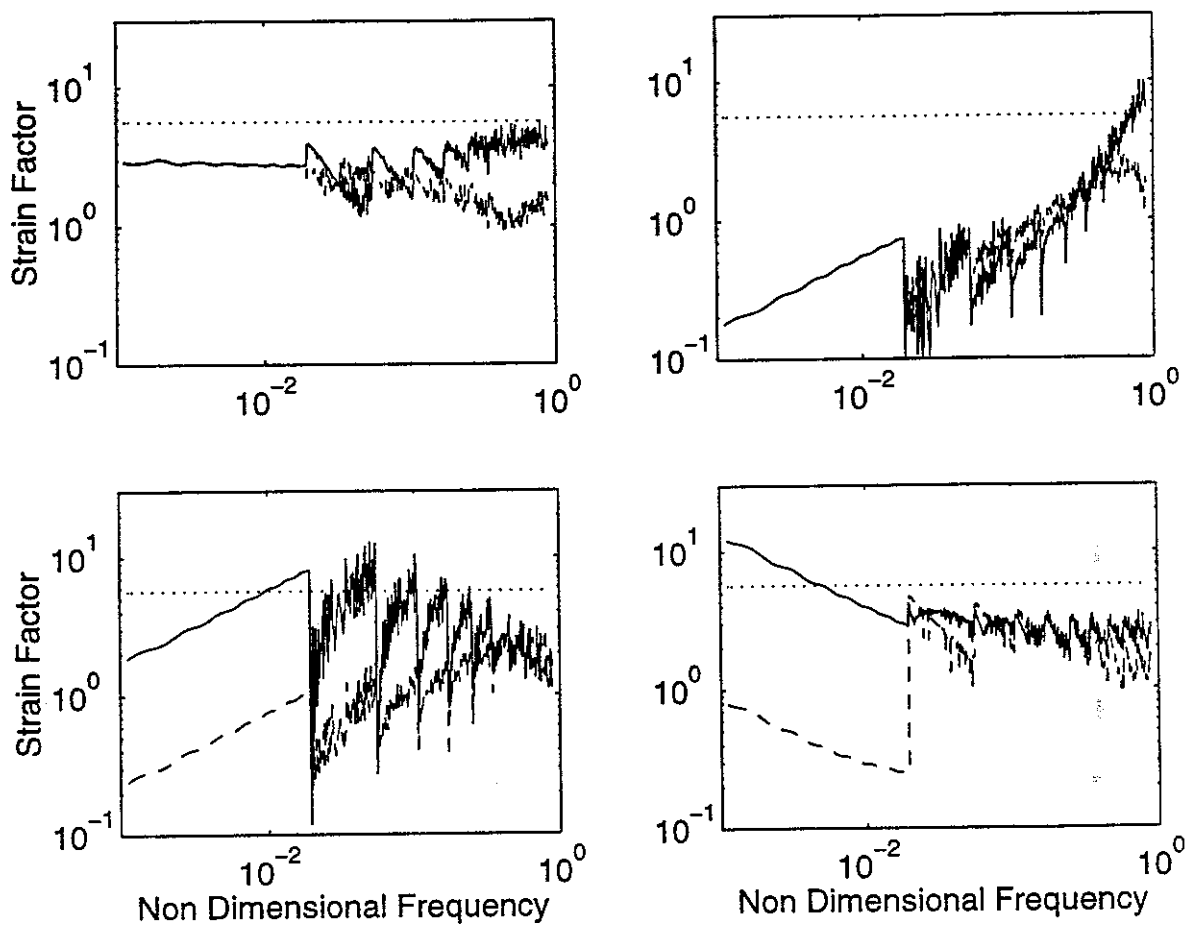

Figure 14 c. Strain Factor for different boundary conditions, $R/T_c = 40$, $\nu = 0.3$; ——, at end; – – –, 1 cm from end; ····; $4\sqrt{2}$; (a), $(u, S_{x\theta}, V_x, M_x)$; (b), (N_x, v, V_x, M_x); (c), $(N_x, S_{x\theta}, w, M_x)$; (d) $(N_x, S_{x\theta}, V_x, w_x)$.

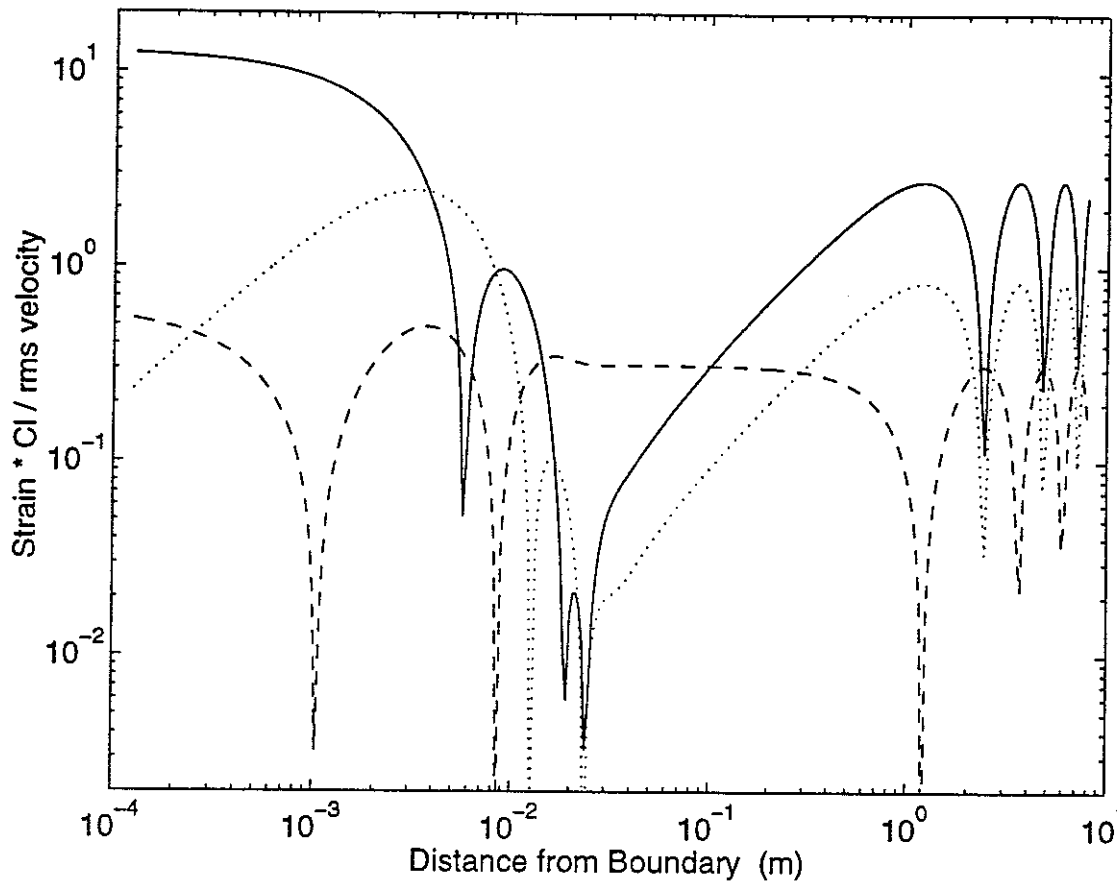

Figure 15. Amplitudes of strain on the outside of the wall in the $n = 1$ beam mode normalised with the ratio of the Sound velocity to the rms radial vibration velocity, $R/T_c = 40$, $\nu = 0.3$, boundary condition (N_x, v, w, w_x), $\Omega = 1.26\,10^{-3}$; —— , axial strain ; $- - -$, shear strain; $\cdots$; circumferential strain.

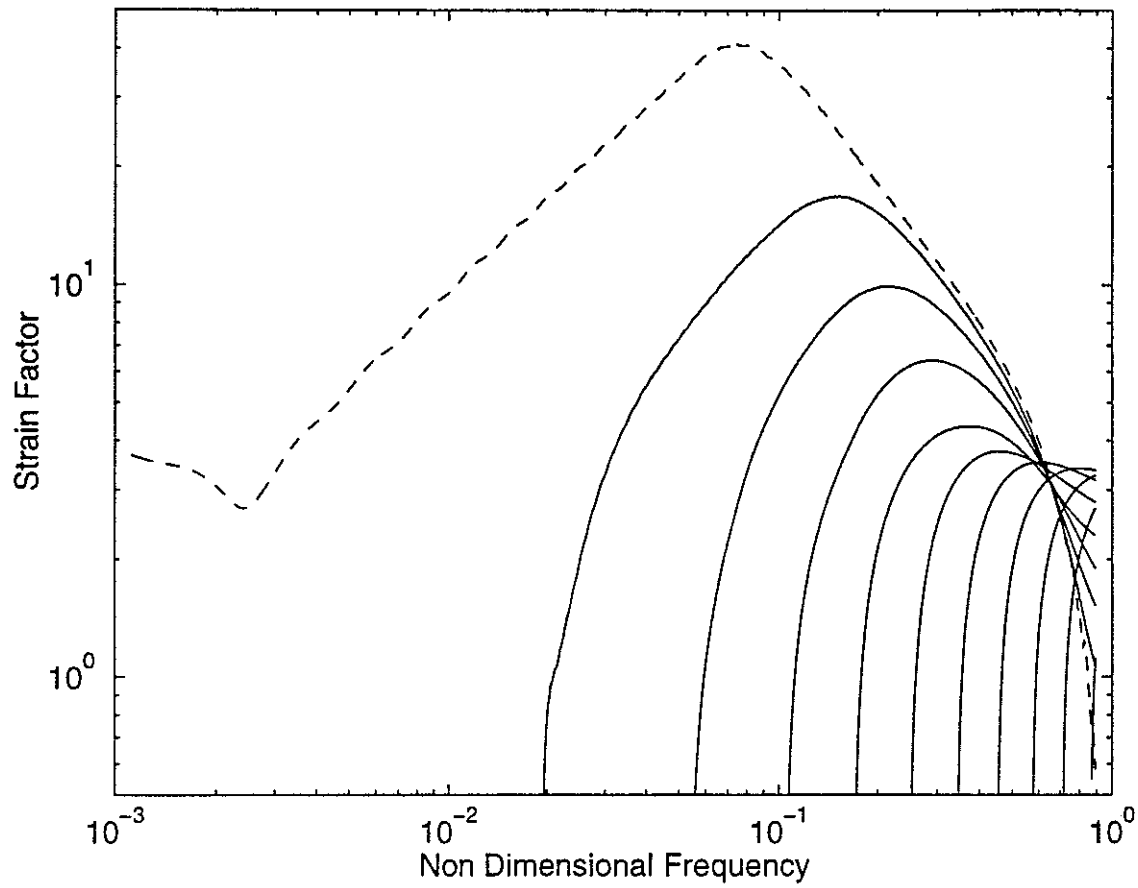

Figure 16. Strain factor for boundary condition $(u, S_{x\theta}, w, M_x)$, $R = T_c / 40$, $\nu = 0.3$; – – –, $n = 1$; ——, $n = 2, 3, .., 12$.

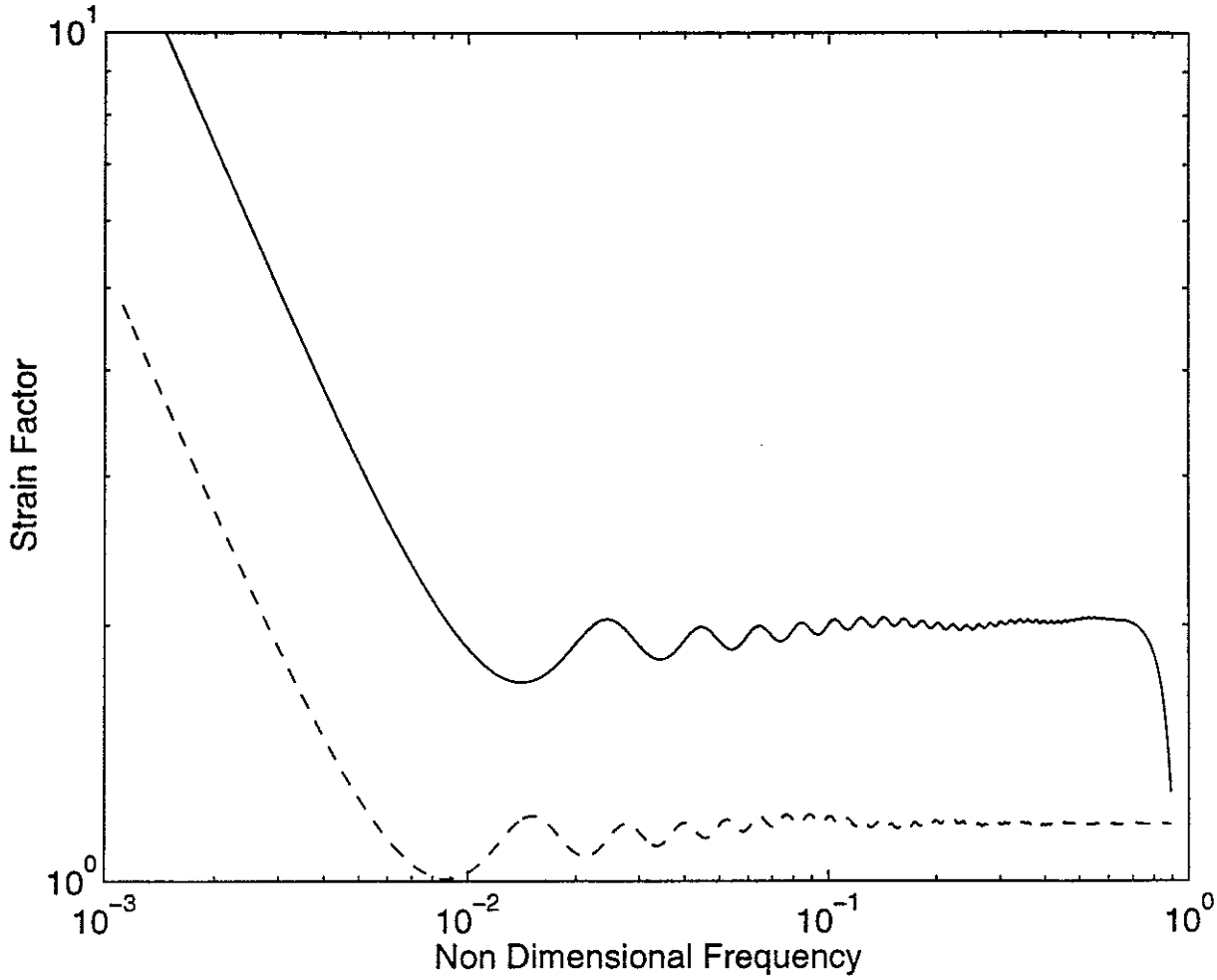

Figure 17. Strain factor at blocked end $R/T_c = 40$, $\nu = 0.3$, $n = 0$; . ——— , axial and radial excitations; – – – –, tangential excitation.

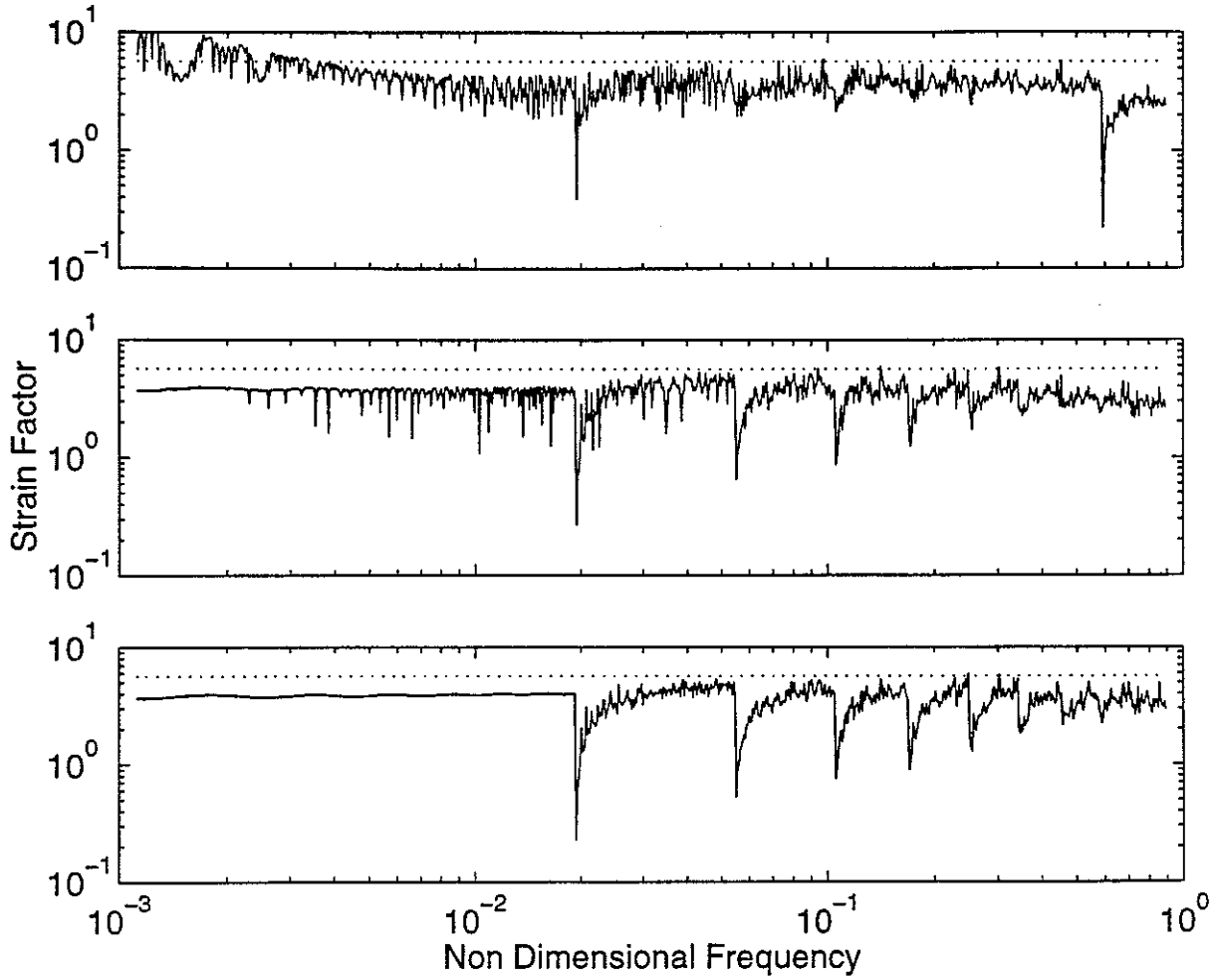

Figure 18. Strain factor at blocked end $R/T_c = 40$, $\nu = 0.3$, $n = 0, 1, \ldots, 16$; . ——, Strain Factor, equation (47); ····; $4\sqrt{2}$; top, axial excitation; middle, tangential excitation; bottom, radial excitation.